In Situ Heparan Sulfate-Induced Peptide Self-Assembly to Overcome the Cell Surface Glycocalyx Barrier for Cancer Treatment

Pengfei Pei,[#] Long Chen,*,[#] Xinyao Guan,[#] Peng Wei, Xiaoxu Kang, Lili Gong, Lihong Liu, Wenxu Guo, Renji Gu, Lixin Wang, Chuanke Zhao,* Jun F. Liang,* and Shi-Zhong Luo*

Cite This: *ACS Appl. Mater. Interfaces* 2024, 16, 49013−49029

Read Online

ACCESS | Metrics & More | Article Recommendations | Supporting Information

ABSTRACT: Heparan sulfate (HS) is a major component of cell surface glycocalyx with extensive negative charges and plays a protective role by preventing toxins, including small molecule drugs and anticancer cationic lytic peptides (ACLPs), from cells. However, this effect may compromise the treatment efficiency of anticancer drugs. To overcome the impedance of cancer cell glycocalyx, an HS-targeting ACLP PTP-7z was designed by fusion of an ACLP and a Zn^{2+}-binding HS-targeting peptide. Upon Zn^{2+} ion binding, PTP-7z could self-assemble into uniform nanoparticles and show improved serum stability and reduced hemolysis, which enable it to self-deliver to tumor sites. The peptide PTP-7z showed a pH- and Zn^{2+} ion-dependent HS-binding ability, which triggers the HS-induced *in situ* self-assembling on the cancer cell surface in the acidic tumor microenvironment (TME). The self-assembled PTP-7z can overcome the impedance of cell glycocalyx by either disrupting cell membranes or translocating into cells through endocytosis and inducing cell apoptosis. Moreover, PTP-7z can also inhibit cancer cell migration. These results proved that HS-responsive *in situ* self-assembling is a practical strategy to overcome the cancer cell glycocalyx barrier for ACLPs and could be extended to the design of other peptide drugs to promote their *in vivo* application.

KEYWORDS: *ACLP, HS targeting, glycocalyx barrier, in situ self-assembling, charge conversion*
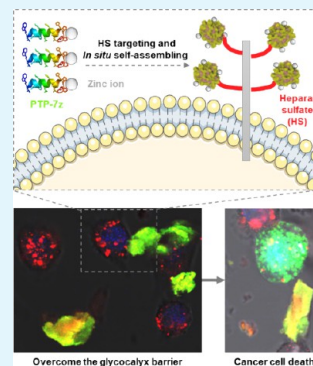
■ INTRODUCTION

Cell surface glycocalyx, which is a dense layer of carbohydrates with plenty of negative charges contributed by heparan sulfate (HS) and sialic acids (SAs), plays important roles in cell physiology, including protecting cells from the accession of a variety of toxins, such as small molecule drugs and anticancer cationic lytic peptides (ACLPs).[1] ACLPs are mainly cationic peptides that interact with the lipid bilayers to damage cell membranes. The interaction between ACLPs and cells starts from the electronic attraction between the cationic peptides and the anionic cell surfaces, which attracts ACLPs to the vicinity of the cells. However, recent studies showed that the negative charges of cell surface glycocalyx might compromise the activity of the ACLPs. Fadnes et al. showed that the negatively charged molecules, especially HS, on the surface of cells inhibited the cytotoxic activity of ACLPs by sequestering them away from the phospholipid bilayer.[2,3] Previous studies of our group also indicated that the increase in the content of surface sialic acid also compromised the cytotoxicity of ACLPs to cells.[4] These research studies demonstrate a contradictory effect of the negative charges of cell surface glycocalyx on ACLPs. Thus, to interact with the cell membrane lipid bilayer, ACLPs must overcome the impedance of glycocalyx.

HS is a major part of the heparan sulfate proteoglycan (HSPG), which is expressed on the surface of all animal cells and is a major component of the extracellular matrix (ECM), mainly consisting of one or more chains of HS that are covalently linked to a core protein. HS is a linear polysaccharide composed of alternating sequences of sulfated disaccharides and highly negatively charged due to the presence of sulfate groups at specific positions. It can interact with a variety of biomolecules, such as growth factors, cytokines, chemokines, morphogens, extracellular matrix proteins, proteases, and protease inhibitors and thus participate in or regulate a variety of physiological processes,[5−7] including endocytosis of macromolecules,[8,9] phase separation,[7] and invasion of viruses.[10,11] For example, when SARS-CoV-2 invades cells, the first step is to bind to HS before binding to ACE2.[12,13] With plenty of negative charges, HS can attract various cations to the vicinity of cells, which play important roles in regulating enzyme activities.[14] Additionally, HS may accumulate cationic cell-penetrating peptides (CPPs) and facilitate them translocating into cells, in which processes peptide aggregation and CPP uptake are correlated.[15] Similarly, the self-assembling and translocating of neuro-degenerative disease-related proteins are also probably mediated by HS.[16−18]
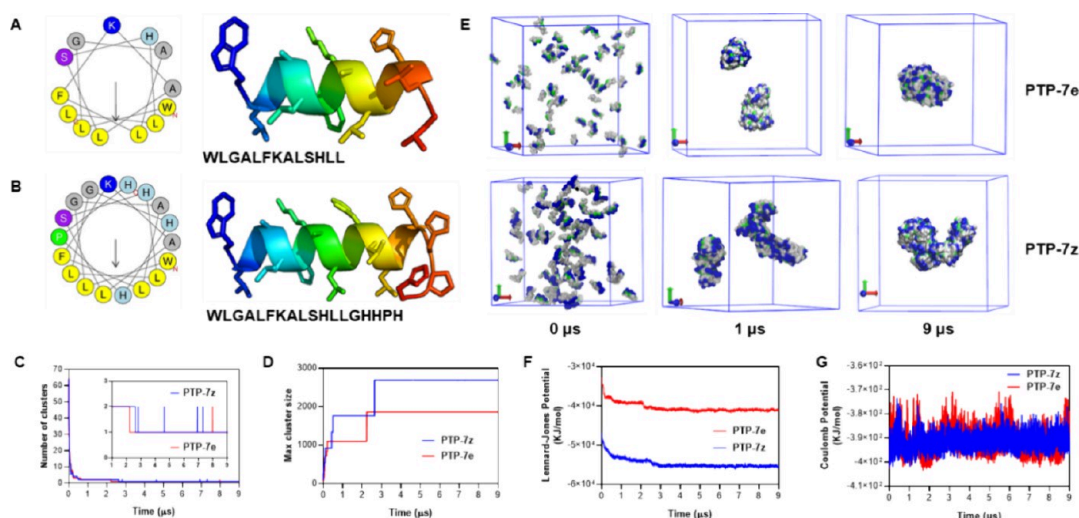
Figure 1. Heparan sulfate (HS) binding peptide design and *in vitro* self-assembling simulation. (A) Helical wheel plots and structure of PTP-7e. (B) Helical wheel plots and structure of PTP-7z. (C) Number of self-assembling clusters and (D) max self-assembling cluster size changes during the simulation process. (E) Snapshots of the peptide self-assemblies at selected time points. Sixty-four peptides were inserted into a $20 \times 20 \times 20$ nm box, and the coloring method is ResType as nonpolar groups in white, basic groups in blue, acidic groups in red, and polar groups in green. (F) Changes of the Lennard-Jones (LJ) potential and (G) Coulomb potential during the simulation process.

In situ self-assembly of proteins or peptides is actually involved in many physiological processes, such as dynamic formation of microtubules. Our previous studies indicated that the disruption of cell membranes by ACLPs also involved *in situ* peptide self-assembling on the lipid bilayer.[19−21] The design of *in situ* self-assembling peptides is also widely applied for diagnosis, induction of immunoreaction, and cell apoptosis for cancer treatment. For example, Wang et al. designed and synthesized a photostable cascade-activatable peptide that can form nanofibers *in situ* on the cell membrane, resulting in long-term and stable imaging of bladder cancer.[18] Li et al. developed a peptide that could self-assemble into nanoscale assemblies in the lysosomes and induced breast cancer cell apoptosis by destroying the mitochondria and cytoskeleton.[22]

Recognizing the roles of HS in peptide interaction with cells, herein, we proposed to design HS-targeted ACLPs that can self-assemble into nanostructures *in situ* on cell surfaces to overcome the impedance of cell glycocalyx via HS-mediated endocytosis to improve the therapeutic applications of ACLPs. Such peptides were constructed by combining an ACLP and an HS-targeting pentapeptide (GHHPH) derived from the core sequence of histidine proline-rich glycoprotein (HPRG). The overall structure of the constructed peptide PTP-7z was amphiphilic to render the self-assembling ability, and binding of Zn^{2+} ions further induced the formation of uniform nanoparticles. With Zn^{2+} ion-improved pH-sensitivity and HS-targeting ability, this peptide could specifically bind to cell surface HS and form *in situ* self-assembly to induce cell membrane disruption and apoptosis at slightly acidic pH (pH 6.5), which fell in the pH range of the tumor microenvironment. The resulted dual modes of action of this peptide for anticancer treatment would converse the role of HS from impedance to facilitation. Meanwhile, the improved serum stability and biosafety make it promising for *in vivo* cancer treatment. The design idea of this peptide provided a useful means to design novel anticancer peptides with targeted therapeutic potentials.

■ RESULTS AND DISCUSSION

Peptide Design and Self-Assembling Simulation. The designed peptide PTP-7z (WLGALFKALSHLLGHHPH) consists of one copy of the consensus sequence (GHHPH) of HPRG, which can bind to transition metals and target heparans,[23] and the aggregating-prone ACLP PTP-7e (WLGALFKALSHLL) derived from a reported peptide PTP-7b.[19] The GHHPH segment with three histidine residues may endow the peptide with pH sensitivity and Zn^{2+} binding ability, enhance the interaction with cell surface HS, and promote endocytosis into tumor cells in the acidic tumor microenvironment (TME).[20] The ACLP segment can promote the self-assembly of the peptide and serve as an effector to lyse cell membranes.

The structures of PTP-7e and PTP-7z were predicted by PEP-FOLD3,[24] which showed that both peptides adopted helical structures with distinct amphiphilic features (Figure 1A,B) that may promote peptide self-assembling in aqueous solution. The peptide self-assembling process was predicted by molecular dynamics simulation with the MARTINI coarse-grained force field.[25] In general, both PTP-7e and PTP-7z could self-assemble simultaneously, showing a two-step process. At the first step, the peptides quickly formed two large aggregates within 0.6 μs, maintaining about 2 μs, and then the two aggregates merged into one single assembly at 3 μs (Figure 1C,D). At last, PTP-7e formed a spherical structure, while PTP-7z formed a fibril structure (Figure 1E), which should be due to their different distributions of polar and hydrophobic residues. The driving force of the peptide self-assembling was mainly van der Waals force as only Lennard-Jones potential was observed to dramatically decline during the self-assembling process (Figure 1F,G), which is similar to those of some reported ACLPs.[21] These results indicate that the designed peptide is able to self-assemble into some specific nanostructures, which preliminarily meets the design idea.

Characterization of the pH- and Zn^{2+}-Responsive Self-Assembling. Histidine is a common transition metal coordination residue that appears in many important motifs of proteins,[26] such as the zinc finger structure,[27−29] and plays an
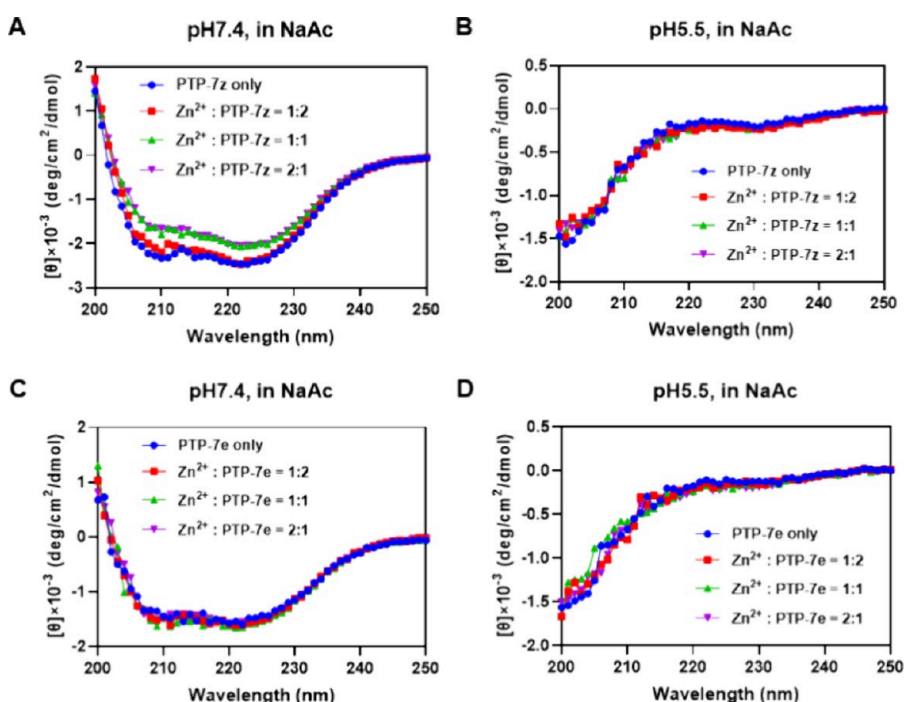
Figure 2. CD spectra of the peptides PTP-7z and PTP-7e. (A, B) CD spectra of PTP-7z in a NaAc solution at pH 7.4 (A) and 5.5 (B). (C, D) CD spectra of PTP-7e in a NaAc solution at pH 7.4 (C) and 5.5 (D). The peptide stock solutions were diluted to 20 μM in 20 mM NaAc with different ratios of zinc ions (Zn^{2+}) at pH 7.4 and 5.5. Data were converted to mean residue molar ellipticity $[\theta]$ [degrees/(cm^2 dmol^{-1})] for each measurement.
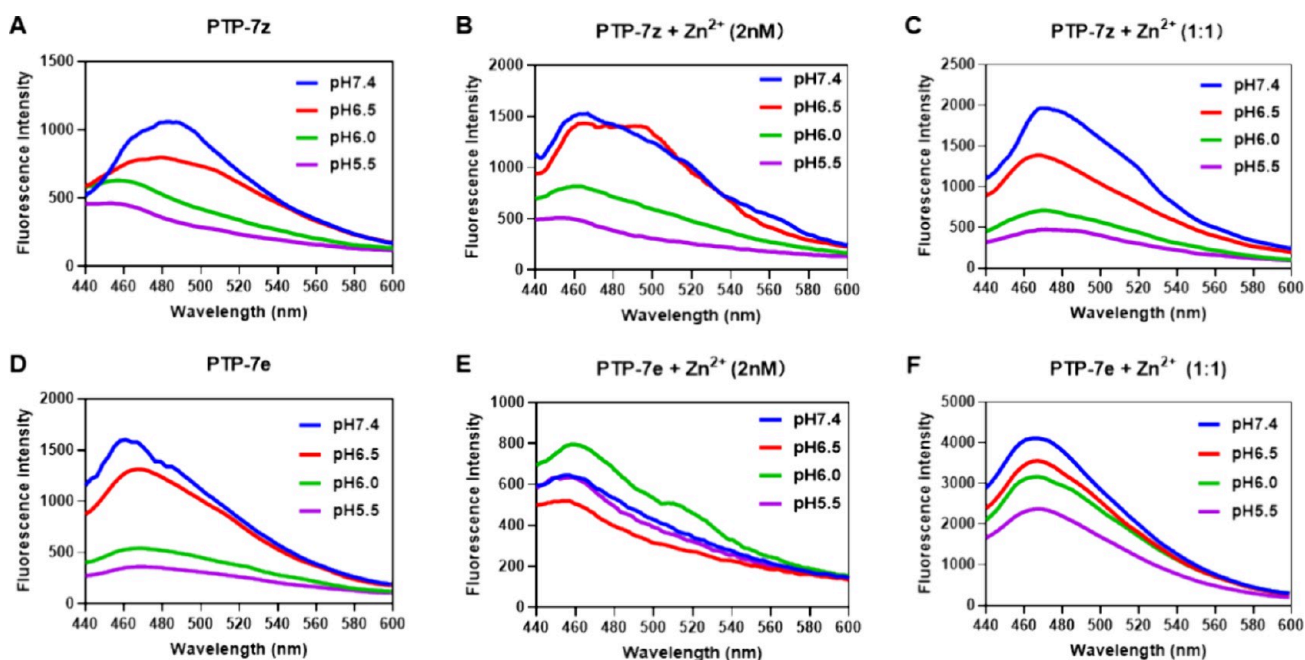

Figure 3. ANS spectra of the peptides at different pH values and Zn^{2+} concentrations. (A−C) ANS spectra of PTP-7z (A) without Zn^{2+} ions and (B) with a low concentration of Zn^{2+} ions (2 nM) or (C) a high concentration of Zn^{2+} ions (1:1 ratio). (D−F) ANS spectra of PTP-7e (D) without Zn^{2+} ions and (E) with a low concentration of Zn^{2+} ions (2 nM) or (F) a high concentration of Zn^{2+} ions (1:1 ratio). Peptide concentration: 80 μM.

important role in exerting protein functions. The repeated consensus sequence $(GHHPH)_n$ (n = 1−3) of HPRG was reported to be able to bind to Zn^{2+} ions[23,30,31]; thus, the Zn^{2+}-binding effect of PTP-7z was first studied. Interaction between the peptides and Zn^{2+} ions was monitored by quenching the intrinsic fluorescence of tryptophan (W). At the physiological

pH (pH 7.4), addition of Zn^{2+} ions caused a sharp and obvious decrease in the intrinsic fluorescence of PTP-7z and a slight decrease in PTP-7e fluorescence. Beyond the peptide/Zn^{2+} ratio of 1.0, the fluorescence of PTP-7z was not further quenched (Figure S1A), while the fluorescence quenching of PTP-7e ceased beyond the ratio of 4.0 (Figure S1D). These
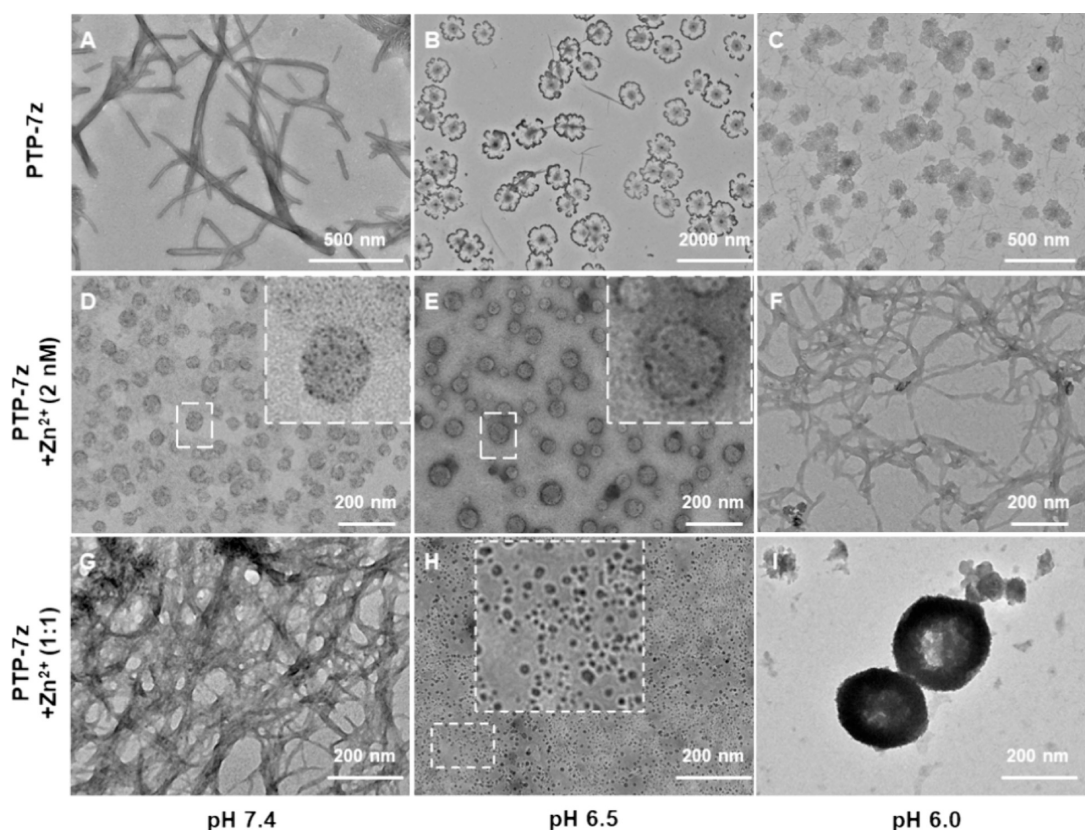
Figure 4. TEM characterization of the pH- and Zn^{2+}-responsive morphology transitions of PTP-7z. (A−C) TEM images of PTP-7z at pH 7.4 (A), 6.5 (B), and 6.0 (C). (D−F) TEM images of PTP-7z in the presence of Zn^{2+} (2 nM) at pH 7.4 (D), 6.5 (E), and 6.0 (F). (G−I) TEM images of PTP-7z in the presence of Zn^{2+} (concentration ratio, 1:1) at pH 7.4 (G), 6.5 (H), and 6.0 (I). The peptide concentration was 80 μM. The boxes show the self-assembly after being enlarged by 4 times.

results indicate that the GHHPH fragment endows PTP-7z with the specific binding ability to Zn^{2+} ions, while the interaction between PTP-7e and Zn^{2+} ions was nonspecific, as it needs more Zn^{2+} ions to quench the tryptophan fluorescence. By contrast, the intrinsic fluorescence of both PTP-7z and PTP-7e was not affected by Zn^{2+} ions at pH 5.5, which should be due to the protonation of the histidine side chain, and thus, they cannot bind to Zn^{2+} ions stably.

At pH 7.4, PTP-7z adopted an α-helix structure in an aqueous NaAc solution, and by adding Zn^{2+} ions, the ratio of the two negative peaks ($[\theta]_{222}/[\theta]_{208}$) in the CD spectra of PTP-7z changed obviously when the concentration of Zn^{2+} ions increased (Figure 2A), which suggests that PTP-7z may form a coiled coil structure after adding Zn^{2+} ions.[32−34] However, the structure of PTP-7z changed to random coil at pH 5.5 and the addition of Zn^{2+} ions showed no effect on its secondary structure (Figure 2B), which was also due to the protonation of the imidazole group of histidine, suggesting that it cannot coordinate with Zn^{2+} ions at this pH. For the peptide PTP-7e, it also adopted an α-helix structure at pH 7.4, which is consistent with its parent peptide PTP-7b.[35] However, the $[\theta]_{222}/[\theta]_{208}$ ratios showed no obvious change when adding Zn^{2+} ions (Figure 2C). Similarly, the structure of PTP-7e also changed to random coil at pH 5.5, and Zn^{2+} ions had no effect on its structure either (Figure 2D). These results further confirm that the GHHPH segment endows the Zn^{2+} ion-binding capacity of PTP-7z, and Zn^{2+} ions may affect the secondary structure and, thus, the self-assembly of PTP-7z at physiological pH.

As suggested by the CD spectra that Zn^{2+} ions may induce coiled coil formation of PTP-7z, the Zn^{2+}-induced peptide self-assembling was further detected by 8-anilino-1-naphthalene-sulfonic acid (ANS) fluorescence, which strongly binds to the cationic group (R, K, and H residues) of proteins and peptides through ion pair formation.[36,37] The measured pH in tumor tissues is typically acidic, and the pH value as low as 5.6 has been measured in human tumors.[38] In most tumors, the pH on surfaces that consisted of highly metastatic cells was around 6.1 to 6.5, whereas in nonmetastatic tumors, the pH was in the range of 6.5−6.9.[39] Therefore, the ANS fluorescence characterization of the peptide self-assembling was performed under pH 7.4, 6.5, 6.0, and 5.5, and pH 6.5 was selected to simulate the acidity of the tumor microenvironment in the characterizations, activity tests, and mechanism studies of the peptides.

The aggregation of pure PTP-7z occurred to some extent at pH 7.4 and 6.5, and the aggregation level decreased as the pH decreased, especially when the pH value was below 6.0, as the aggregation ability of PTP-7z was nearly lost (Figure 3A). Since the histidine residues in PTP-7z could be protonated as the pH decreased, the resulting electrostatic repulsion between the PTP-7z monomers would induce dis-assembling of the self-assemblies, which results in the fluorescence decrease of ANS. When adding a low concentration of Zn^{2+} ions at 2 nM, a concentration that can significantly affect HPRG−heparin interaction at physiological pH,[23] the aggregation of PTP-7z was enhanced at pH 7.4 and 6.5, manifesting as increased fluorescence intensity (Figure 3B). Moreover, the fluorescence intensity at pH 6.5 in Figure 3B was higher than that in Figure
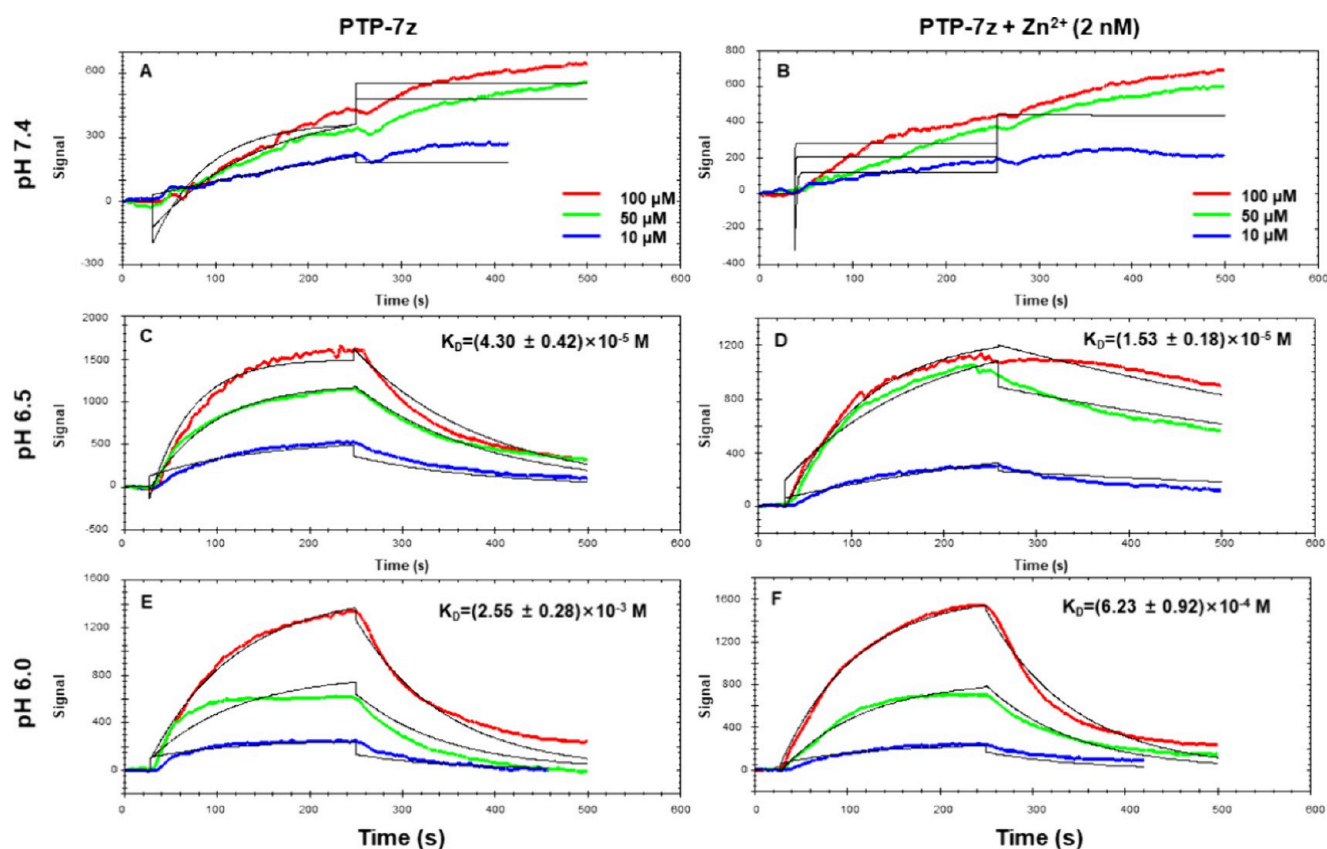
Figure 5. pH- and Zn^{2+}-dependent binding kinetics of PTP-7z to HS determined by surface plasmon resonance (SPR). (A, C, E) Binding kinetics of PTP-7z to HS in PBS at pH 7.4 (A), 6.5 (C), and 6.0 (E). (B, D, F) Binding kinetics of PTP-7z to HS in PBS containing Zn^{2+} (2 nM) at pH 7.4 (B), 6.5 (D), and 6.0 (F). For the PTP-7z group, 1× PBS at different pH values was used as running buffer. For the PTP-7z + Zn^{2+} (2 nM) group, 1× PBS with 2 nM Zn^{2+} at different pH values was used as running buffer.

3A, suggesting that Zn^{2+} ions (even at concentrations as low as 2 nM) could enhance the self-assembling of PTP-7z. At the Zn^{2+}/peptide ratio of 1.0, the aggregation of PTP-7z at pH 7.4 was enhanced once again, which showed higher ANS fluorescence intensity (Figure 3C) that may come from the enhanced histidine−Zn^{2+} interaction. The fluorescence intensity at pH 6.5 in Figure 3C was not higher than that in Figure 3B, suggesting that the Zn^{2+} ion binding ability may be limited to a certain level at pH 6.5 due to the electrostatic repulsion. Meanwhile, the fluorescence intensity at pH 5.5 and 6.0 in Figure 3B,C was similar to that in Figure 3A, suggesting that the electrostatic repulsion comes from significant histidine-protonation-induced dis-assembling and cannot be compensated by the Zn^{2+} enhancement.

The aggregation of PTP-7e was stronger than that of PTP-7z at pH 7.4 and 6.5 (Figure 3D), which may be due to the overall higher hydrophobicity of PTP-7e. At the Zn^{2+}/PTP-7e ratio of 1.0, the ANS fluorescence intensity was almost two times as that of PTP-7z at pH 7.4 and 6.5 and even much higher at pH 6.0 and 5.5 (Figure 3F), suggesting that the Zn^{2+} strength has stronger impact than pH change for the self-assembling of PTP-7e, as the only histidine residue in PTP-7e may not induce enough electrostatic repulsion. The stronger impact of Zn^{2+} strength also caused the abnormal fluorescence of PTP-7e when the concentration of Zn^{2+} was 2 nM, as the highest fluorescence appeared at pH 6.0 and the lowest at pH 6.5 (Figure 3E). This result suggests that ANS may bind to the external sites of the self-assembly under this condition,[40] since ANS located in the buried binding site that exhibits long-

lifetime fluorescence is not accessible to the water molecules, while ANS from the sites demonstrating short-lifetime fluorescence is accessible to water molecules.[41] Further detection of the time-dependent fluorescence decay at pH 6.0 and 5.5 confirmed this conjecture (Figure S2B,C).

Moreover, there was a peak shift in addition to the fluorescence intensity change, which should come from the positive charge increase of the peptides that alters the fluorescence emission maximum of ANS, since the sulfonate group in ANS interacts with the positively charged amino acids,[42] and this interaction may alter intra- and intermolecular charge transfer processes that define the fluorescence emission maximum and lifetime of ANS.[40] On the other hand, it has been suggested that both the restricted mobility and hydrophobicity of the nearest environment of ANS contribute significantly to the peak shift of the fluorescence spectra and fluorescence intensity.[40,41] The pH-dependent morphology transformations of the peptide self-assemblies that changed the environment of the ANS binding site may also contribute to the peak shift.

The self-assembling nanostructures of PTP-7z were observed by electron microscopes. The morphology of PTP-7z self-assembly at pH 7.4 was tube-like with a diameter of ∼20 nm in the TEM images (Figure 4A), and the tubes were spiral in the SEM images (Figure S3), which may come from the formation of a coiled coil. As the pH value decreased to 6.5, the morphology of the PTP-7z self-assembly changed to a flower-like shape with a dense core and a petal-like shell (Figure 4B). At pH 6.0, the petal-like shell disappeared and
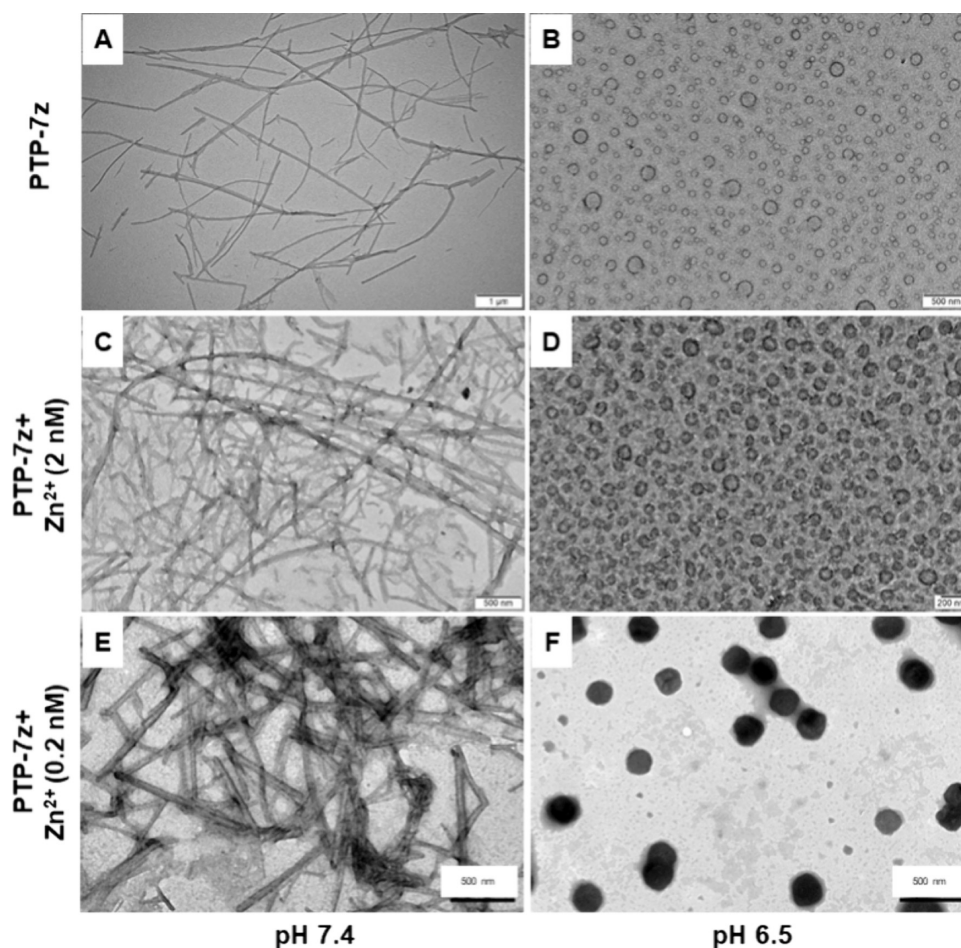
Figure 6. TEM images of the PTP-7z assemblies and PTP-7z-Zn^{2+} coassemblies after stimulation by HS. (A, B) TEM images of the PTP-7z assemblies after stimulation by HS at pH 7.4 (A) and 5.5 (B). (C, D) TEM images of the PTP-7z + Zn^{2+} (2 nM) coassemblies after stimulation by HS at pH 7.4 (C) and 5.5 (D). (E, F) TEM images of the PTP-7z + Zn^{2+} (0.2 nM) coassemblies after stimulation by HS at pH 7.4 (E) and 5.5 (F). HS at 250 μg/mL was used to stimulate the PTP-7z-Zn^{2+} coassemblies.

more short fibers appeared around the dense core particles (Figure 4C). These results might indicate the process of self-assembly collapse when solution pH decreases.

Addition of Zn^{2+} ions caused an obvious change in the morphology of the PTP-7z self-assembly. When 2 nM Zn^{2+} ions were added to PTP-7z, the nanotubes collapsed to small nanoparticles with a diameter of ∼50 nm at pH 7.4 (Figure 4D), and the size and morphology of PTP-7z self-assembly showed no obvious change at pH 6.5 (Figure 4E), but it reassembled into nanofibers at pH 6.0 (Figure 4F). However, when the concentration of Zn^{2+} ions was at a high level (1:1 to the peptide), PTP-7z formed highly cross-linked fibers at pH 7.4 (Figure 4G) but collapsed into a spherical structure at pH 6.5 (Figure 4H) and finally into hollow spheres with diameters of ∼200 nm at pH 6.0 (Figure 4I). The morphology of the peptide self-assembly could have a significant influence on the biodistribution, release, and pharmacokinetics profile of ACLPs,[34,43−45] and the diversity of PTP-7z self-assembly morphology under various pH values and Zn^{2+} concentrations provides more choices for its pharmaceutical preparation.

The stability of bioactive peptides in circulation is usually low due to the clearance of the kidney and degradation by various proteases. We previously proposed that peptide self-assembling could improve the stability of peptides in serum and protect them from proteases, thus leading to elongated

circulation *in vivo*.[20] As it was previously indicated that Zn^{2+} ions could enhance PTP-7z self-assembling, we tested the serum stability of these peptides by HPLC. The half-life of pure PTP-7z in serum was about 0.5 h, and in the presence of Zn^{2+} ions, the half-life of PTP-7z was also obviously increased, which was 1.18 and 4.27 h at low and high concentrations of Zn^{2+} ions, respectively (Figure S4A). In contrast, the peptide PTP-7e was quite unstable in serum, since it was fully degraded in about 0.1 h (Figure S4B). In the presence of Zn^{2+} ions, the half-lives of PTP-7e in serum increased to 0.68 and 0.88 h at low and high concentrations of Zn^{2+} ions, respectively. Although Zn^{2+} ions improved the serum stability of PTP-7e, the half-lives were still not satisfied for *in vivo* application. These results indicate that Zn^{2+} ions can improve the stability of PTP-7z, and the increased half-lives may make it applicable *in vivo*.

The hemolysis of PTP-7z was also tested, as it was derived from a lytic peptide. PTP-7z can cause obvious hemolysis only at concentrations as high as 500 μM and even no obvious hemolysis at this concentration in the presence of Zn^{2+} ions (Figure S4C). However, PTP-7e caused dramatic hemolysis even at 62.5 μM. Although the hemolytic effect of PTP-7e was alleviated in the presence of Zn^{2+} ions, hemolysis was restored at 250 μM (Figure S4D). The decrease in hemolysis at 500 μM of PTP-7e might come from the aggregation of the peptide at
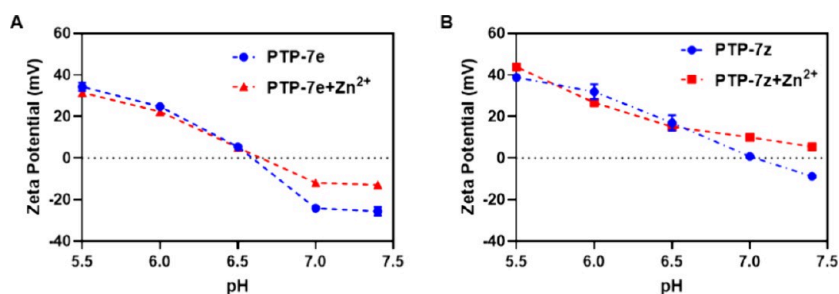
Figure 7. pH-responsive charge conversion of the peptides. (A) Zeta potentials of peptides PTP-7z and (B) PTP-7e at different pH values. The Zn^{2+}/peptide ratio in the ion addition group was 1.0 for both peptides.

high concentrations. Such improved serum stability and reduced hemolysis of PTP-7z in the presence of Zn^{2+} ions might come from the Zn^{2+}-enhanced peptide self-assembly, as some proteolytic sites in the sequence and the hydrophobic residues, which are prone to cause hemolysis, are buried inside the self-assembly.

pH- and Zn^{2+}-Dependent HS Binding of the Peptides. It has been reported that the targeting peptide (GHHPH) is able to bind HS in a pH- and Zn^{2+}-dependent manner.[23] To further confirm the targeting ability of PTP-7z to HS, the binding of PTP-7z to HS was determined by surface plasmon resonance (SPR) at different pH values and in the presence of Zn^{2+} ions (2 nM). At pH 7.4, PTP-7z showed no binding to HS, even after the addition of Zn^{2+} ions (Figure 5A,B). When the pH decreased to 6.5, the binding ability of PTP-7z to HS was significantly enhanced, with an affinity constant $K_D = (4.30 \pm 0.42) \times 10^{-5}$ M (Figure 5C), and the binding ability was further enhanced after the addition of Zn^{2+}, with the K_D reduced to $(1.53 \pm 0.18) \times 10^{-5}$ M (Figure 5D). This pH- and Zn^{2+}-dependent HS targeting of PTP-7z should come from the increased charges by protonation and Zn^{2+} binding, which was similar to the GHHPH consensus sequence.[23] However, when the pH was further reduced to 6.0, the HS-binding ability of PTP-7z weakened compared to that at pH 6.5, with the $K_D = (2.55 \pm 0.28) \times 10^{-3}$ M (Figure 5E) for PTP-7z alone and $K_D = (6.23 \pm 0.92) \times 10^{-4}$ M (Figure 5F) in the presence of Zn^{2+}, which may come from the structural flexibility of the peptide at pH 6.0. By contrast, the peptide PTP-7e showed weak binding to HS (Figure S5), even at acidic pH and in the presence of Zn^{2+}. The binding ability of PTP-7e to HS was much lower than that of PTP-7z, which was due to the absence of the targeting sequence GHHPH. However, HS may also adsorb some PTP-7e peptides, because HS bears a large number of negative charges, which causes some nonspecific binding to the positively charged peptide. These results indicate that PTP-7z shows pH- and Zn^{2+}-dependent binding to HS, which could be ideal for HS-targeted anticancer treatment. Therefore, the desired self-assembling and HS-targeting abilities of the designed peptide PTP-7z were both realized.

Moreover, the effect of HS on the self-assembling structure of PTP-7z was further observed. The HS-stimulated samples were prepared by adding HS at 250 μg/mL, as the self-assembling behavior could be significantly changed at this concentration (Figure S6A,B), to the self-assemblies prepared as in Figure 4. For the pure PTP-7z peptide, the stimulation of HS made it form longer fibers at pH 7.4 (Figure 6A) and denser nanoparticles at pH 6.5 (Figure 6B). Interestingly, with HS addition, the structure of the PTP-7z + Zn^{2+} ions (2 nM) sample changed from nanoparticles (Figure 4D) to dense

fibers (Figure 6C), which may due to the deprivation of Zn^{2+} ions by HS. At pH 6.5, HS only extended the size of the nanoparticles of the PTP-7z + Zn^{2+} ions (2 nM) sample (Figures 4E and 6D).

The normal plasma concentration of free Zn^{2+} is about 0.2 nM.[46] The effect of this low concentration of Zn^{2+} to the HS-responsive assembly of PTP-7z was also tested. ANS fluorescence indicated that the self-assembling of PTP-7z at pH 7.4 was similar when the Zn^{2+} concentrations were 0.2 and 2 nM (Figure S6C), while there was a difference at pH 6.5 (Figure S6D). The morphology was also fibers at pH 7.4 (Figure 6E) and nanoparticles at pH 6.5 (Figure 6F). In general, the HS-responsive self-assembling of PTP-7z was observed, and the stimulation of HS changed the self-assembly morphologies, which suggested that the HS-mediated *in situ* PTP-7z self-assembling could be achieved. Moreover, since fibrous nanostructures persist longer in circulation,[45] the HS-stimulated fiber assemblies at pH 7.4 could increase the *in vivo* stability of PTP-7z. The spherical nanostructures are easier to be taken up by the cells than fibrous nanostructures[44]; thus, the HS-stimulated nanospheres of PTP-7z at pH 6.5 could facilitate endocytosis by the cancer cells.

Charge Conversion of the Peptides. As described above, the self-assembling and HS targeting were both pH- and Zn^{2+} ion-dependent, which are closely related to the charging state of the peptide. Moreover, the charging state of ACLPs is essential to their interaction with cells, and the pH-responsive cytotoxicity of histidine-containing ACLPs has been previously reported, which is due to the charge conversion of the histidine side chains at acidic pH values, whose pK_a is 6.0. Thus, the His residue acts as a charge switch because it can be protonated to bear a positive charge at acidic pH values. For example, the parent peptide (PTP-7b) of PTP-7e and PTP-7z has been reported to have a pH sensitivity of 3.0 on A549 cells, which means that its activity at acidic pH is 3-fold that at physiological pH.[35]

Because of the importance of the charging state of histidine, the charge conversion of the peptide PTP-7z induced by acidic pH and the Zn^{2+} ion was determined. By measuring the zeta potentials of the peptides at various pH values, it can be found that both PTP-7z and PTP-7e took negative charges at physiological pH (pH 7.4) but reversed to positive charges at acidic pH values (Figure 7). The charge conversion of PTP-7e occurred at about pH 6.5 (Figure 7A), while the charge conversion point of PTP-7z was about pH 7.0 (Figure 7B). This might be because PTP-7z has more histidine residues than PTP-7e, and the microenvironments of the histidine residues in PTP-7z are much different. Upon addition of Zn^{2+} ions, the zeta potentials of both peptides increased at pH 7.4
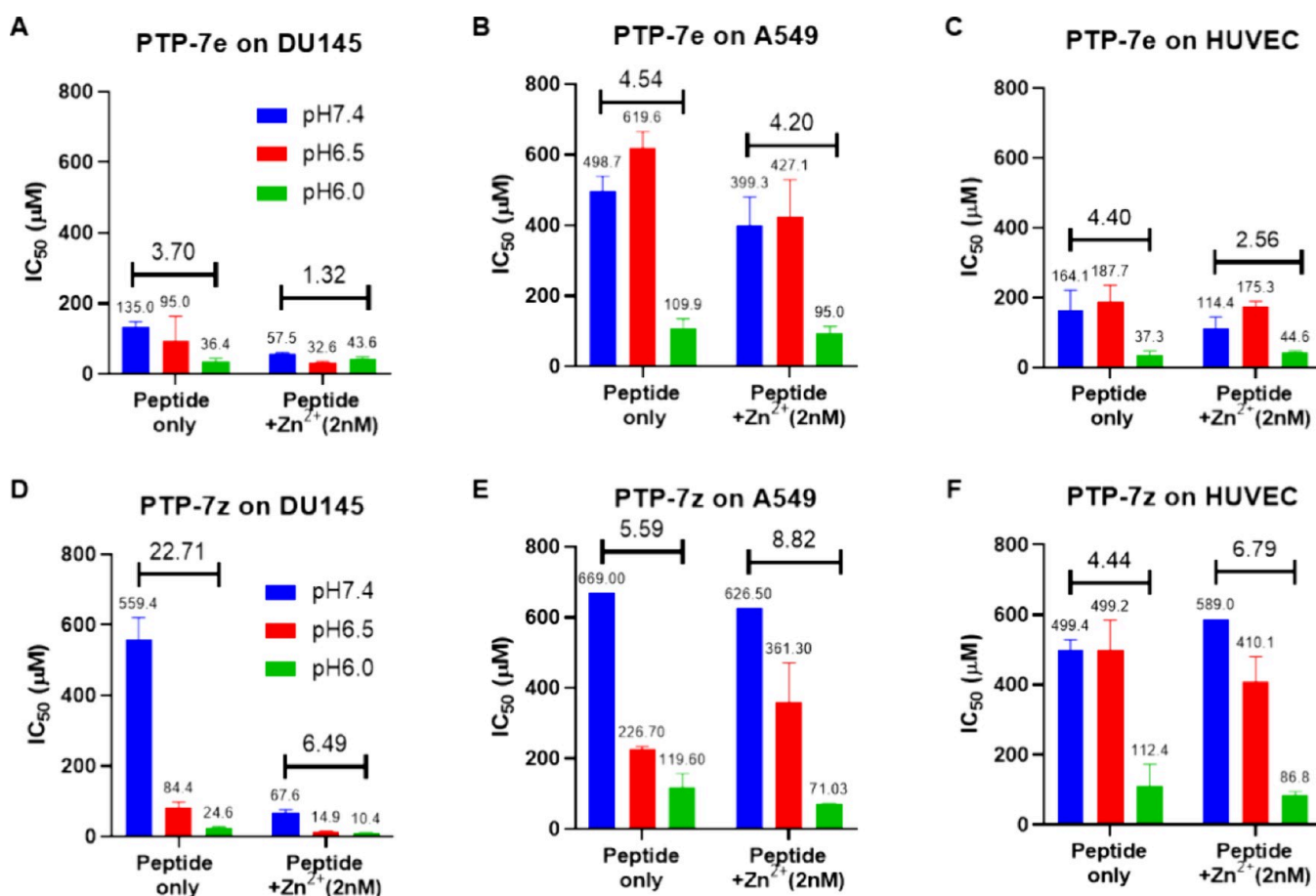
Figure 8. Cytotoxicity IC_{50} of PTP-7e and PTP-7z on DU145, A549, and HUVEC cell lines. (A–C) Cytotoxicity IC_{50} of PTP-7e and PTP-7e with Zn^{2+} (2 nM) under pH 7.4, 6.5, and 6.0 on the DU145 (A), A549 (B), and HUVEC (C) cell lines. (D–F) Cytotoxicity IC_{50} of PTP-7z and PTP-7z with Zn^{2+} (2 nM) under pH 7.4, 6.5, and 6.0 on the DU145 (D), A549 (E), and HUVEC (F) cell lines. The pH-sensitivity value was calculated as the ratio of the IC_{50} value at pH 7.4 to that at pH 6.0 and labeled on the line with text.

and 7.0, and it even caused charge conversion of PTP-7z at these pH values. By contrast, Zn^{2+} ions did not obviously affect the charges of the peptides at acidic pH values, which is consistent with the protonation of histidine residues. This could explain why the Zn^{2+} ions improved the HS binding of PTP-7z as Zn^{2+} ion complexation increased its zeta potentials. Further considering the SPR results, pH 6.5–7.0 seems to be the best pH range for the HS binding of the PTP-7z-Zn^{2+} complex because the positive charges at pH values above 7.0 are not sufficient enough for HS binding, while the structure of PTP-7z at pH values lower than 6.5 is too flexible to bind to HS specifically. Since the microenvironment of solid tumors is acidic and usually falls in the pH range of 6.4–7.0,[38] the PTP-7z-Zn^{2+} complex is ready to target HS in such an acidic tumor microenvironment (TME).

pH- and Zn^{2+} Ion-Enhanced Cytotoxicity of PTP-7z. The pH-activated cytotoxicity of PTP-7z and PTP-7e was first examined (Figures S8–S10), as their parent peptide PTP-7b showed definite pH sensitivity due to the histidine residue in the sequence.[19,20] PTP-7e exhibited obvious pH-enhanced cytotoxicity against all three tested cell lines (DU145, A549, and HUVEC), as its pH sensitivity on all these cell lines was more than 3.7 (Figure 8A–C), which was calculated as the ratio of the IC_{50} value at pH 7.4 to that at pH 6.0, because the histidine residue was considered to be fully protonated at pH 6.0.[35] This enhanced cytotoxicity with decreasing pH is

consistent with its charge conversion, as the protonation state of histidine changed, and agreed with its parent peptide PTP-7b.[19,20] By contrast, PTP-7z showed higher pH sensitivity on these three cells, and the greatest pH sensitivity was about 22.7 on DU145 (Figure 8D–F), which should be because PTP-7z contains more histidine residues. This much higher pH sensitivity on DU145 cells could be affected by the interaction between PTP-7z and HS, as DU145 has a high HS level on cell surfaces.[47]

The activities of the peptides in the presence of Zn^{2+} ions were tested only at 2 nM Zn^{2+} ions in the following experiments, considering the cytotoxicity of Zn^{2+} ions at high concentrations (Figure S7). In addition, the peptides with a low concentration (2 nM) of Zn^{2+} ions can self-assemble into nanoparticles (Figure 4D), which are more homogeneous and stable in solution than nanofibers.[34] Moreover, 2 nM Zn^{2+} ions can efficiently enhance the HS binding of PTP-7z so that the effect of HS on the cytotoxicity of the peptides can be further evaluated under this condition. The premixture of PTP-7z and Zn^{2+} ions obviously increased the cytotoxicity of PTP-7z on DU145 cells in comparison to that without Zn^{2+} ions, especially at pH 6.5 (Figure 7D), which might come from the enhanced HS binding at this pH, as shown in the SPR experiment (Figure 5C,D). However, the activity of PTP-7z in the presence of Zn^{2+} ions at pH 6.0 just improved slightly, which might be because the protonated peptide cannot bind to
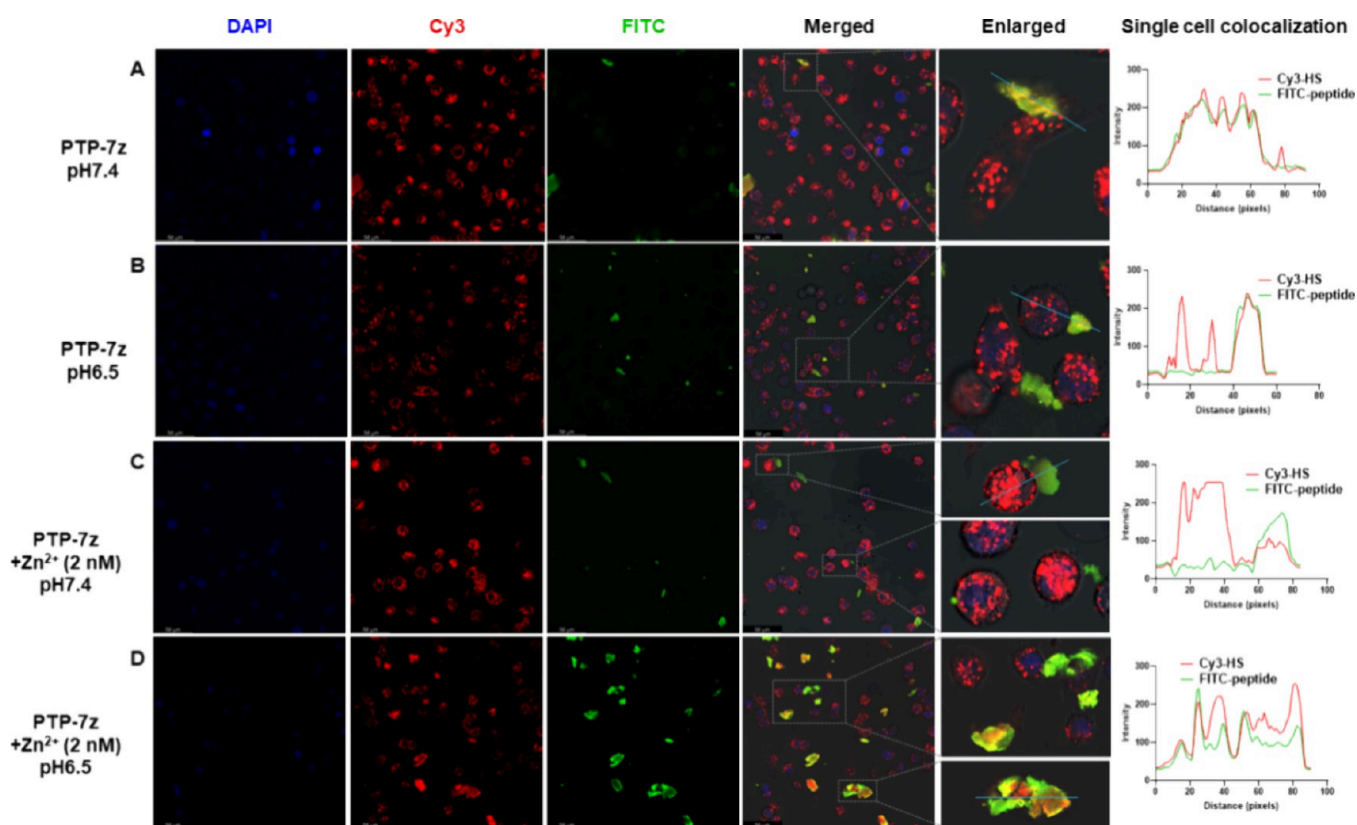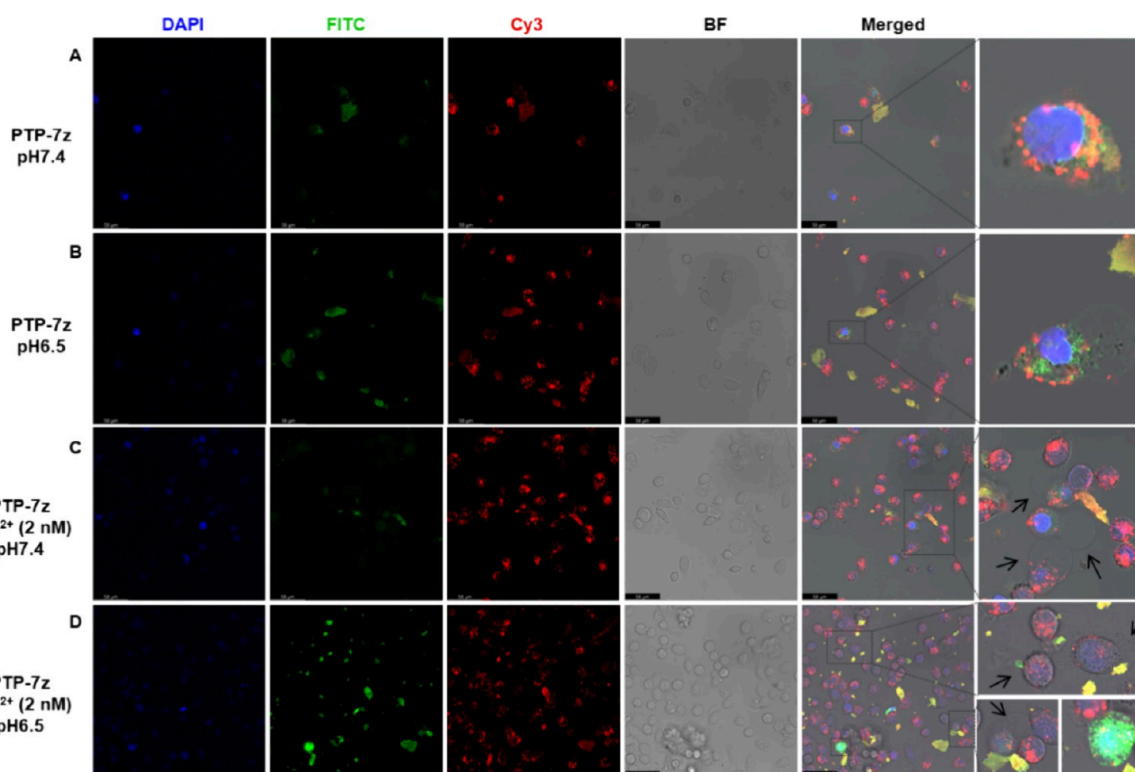
Figure 9. pH- and Zn^{2+}-dependent targeting of PTP-7z to cell surface HS that was detected by confocal laser scanning microscopy (CLSM) imaging. (A) CLSM images of PTP-7z-treated DU145 cells at pH 7.4. (B) CLSM images of PTP-7z-treated DU145 cells at pH 6.5. (C) CLSM images of DU145 cells treated with PTP-7z combined with Zn^{2+} (2 nM) at pH 7.4. (D) CLSM images of DU145 cells treated with PTP-7z combined with Zn^{2+} (2 nM) at pH 6.5. The DU145 nuclei were stained with DAPI (blue), and HS was bound by a primary antibody (10E4) first and then stained with a Cy3-labeled secondary antibody (red). The peptide was labeled with FITC (green). The images were taken after the addition of peptide for 0.5 h. Single-cell colocalization was analyzed by the ImageJ script Plot Profile.

Zn^{2+} ions and just exhibited the activity of the free peptide. By contrast, the Zn^{2+}-enhanced cytotoxicity of PTP-7z on A549 cells was not observed at pH 7.4 and 6.5 and even lowered in the presence of Zn^{2+} ions. However, a slight increase was observed at pH 6.0 (Figure 8E). A plausible explanation is that the HS contents of A549 cells are lower than those of DU145, and the enhanced HS binding may impede peptide accession to cell membranes but cannot trigger HS-mediated cellular translocation. For PTP-7e, addition of Zn^{2+} ions also increased its cytotoxicity, but the increasing amplitude was much smaller (Figure 8A−C), which could be just due to the nonspecific cytotoxicity of Zn^{2+} ions that were brought to the cell membranes by the peptide.

These results suggest that PTP-7z possesses selective anticancer activity, which could be related to its HS-targeting ability endowed by the HS-targeting motif (GHHPH). Both acidic pH and Zn^{2+} ions could enhance the cytotoxicity of PTP-7z, and pH plays a more important role in activating its anticancer activity. The expression level of HS is different in various tumor cell lines, and thus, the HS-targeting peptide showed varied activities on these tumor cells. The non-small cell lung cancer cell line A549 has a low level of HS expression,[23] so the cytotoxicity of PTP-7z is weaker on A549 than that on DU145 cells. Such acidic pH-activated and HS-targeted anticancer activity makes PTP-7z safer in the application of anticancer treatment since its cytotoxicity on the endothelial cell line HUVEC is also weak (Figure 8F). Moreover, PTP-7e showed relatively high cytotoxicity on the

human vascular endothelial cell line HUVEC regardless of the absence or presence of Zn^{2+} ions (IC_{50} = 164.1 and 114.4 μM, Figure 8C).

Anticancer Mechanism of the Peptide PTP-7z. As described above, the peptide PTP-7z was able to bind to HS and may thus affect its cytotoxicity on cancer cells, so the *in situ* interaction between the peptides and cell surface HS was observed by confocal immunofluorescence imaging on DU145 cells. After the cells were incubated with PTP-7z at pH 7.4 for 0.5 h, green fluorescence on some cell surfaces could be observed, and large peptide aggregates that colocalized with HS sparsely appeared (Figure 9A). The number of large PTP-7z-HS colocalized aggregates on cell surfaces was increased when incubating the cells and PTP-7z at pH 6.5 (Figure 9B), suggesting that lower pH can promote HS binding and *in situ* self-assembling of PTP-7z due to the partial charge conversion of the peptides. In the presence of Zn^{2+} ions at pH 7.4, a similar number of PTP-7z-HS aggregates were observed on the cell surfaces (Figure 9C), which might also be caused by charge conversion, as Zn^{2+} binding could increase the positive charges of the peptide complex. In the presence of Zn^{2+} ions at pH 6.5, a large amount of PTP-7z bound to cell surface HS, and the fluorescence color could cover the whole cells and turned more yellow (Figure 9D), indicating that the binding of PTP-7z was largely mediated by cell surface HS and the targeting ability to HS under this condition was the strongest for PTP-7z. In contrast, PTP-7e did not show a strong HS-targeting ability under all conditions (Figure S11). A small

Figure 10. *In situ* self-assembling with HS and membrane lysis of PTP-7z that was detected by confocal laser scanning microscopy (CLSM) imaging. (A) CLSM images of PTP-7z-treated DU145 cells at pH 7.4. (B) CLSM images of PTP-7z-treated DU145 cells at pH 6.5. (C) CLSM images of DU145 cells treated with PTP-7z combined with Zn^{2+} (2 nM) at pH 7.4. (D) CLSM images of DU145 cells treated with PTP-7z combined with Zn^{2+} (2 nM) at pH 6.5. The DU145 nuclei were stained with DAPI (blue), HS was bound by a primary antibody (10E4) first and then stained with a Cy3-labeled secondary antibody (red), and the peptide was labeled with FITC (green). The images were taken after the addition of peptide for 2 h.

number of PTP-7e aggregates were observed in the field of view in the absence of Zn^{2+} ions at pH 6.5 or in the presence of Zn^{2+} ions at both pH values, but colocalization with HS was not evident (Figure S11B–D), whereas no obvious peptide binding was observed in the absence of Zn^{2+} ions at pH 7.4 (Figure S11A). The fluorescence colocalization assay results showed that PTP-7z could actively target HS on the cell membrane, and the targeting ability was enhanced under acidic pH or in the presence of Zn^{2+}, so it is reasonable to believe that HS can nucleate *in situ* PTP-7z self-assembling on the cell surface.

According to the cell lytic mechanism of the parent peptide,[19−21] the membrane lysis caused by these peptides was further examined at an extended period. After addition of the peptide for 2 h, it can be observed that FITC-labeled PTP-7z (green fluorescence) accumulated with the glycocalyx barrier HS at pH 7.4 (Figure 10A). Moreover, since the glycocalyx barrier locates just outside the cell membrane, the fluorescence from the HS-bound Cy3 could indicate the membrane; thus, it can be observed that PTP-7z entered the cancer cells at pH 6.5 (Figure 10B). Cell blebbing and cytoplasmic leakage were also observed (Figure 10B), and they were enhanced in the presence of Zn^{2+} ions (Figure 10C,D). These results suggest that PTP-7z could induce cancer cell lysis, as cell blebbing is a universal cellular response to plasmalemmal injury.[48,49] Moreover, more green fluorescence was observed for the cells treated with PTP-7z at this time point, suggesting that the binding of PTP-7z to HS is time-dependent.

In contrast, for the cells treated with PTP-7e, it can be observed that cells were blebbing under all conditions, while peptide-HS colocalization is rare (Figure S12), which is consistent with the nonspecific cytotoxicity of PTP-7e. This high sensitivity of cytotoxicity change at near physiological pH could be more beneficial for cancer treatment using PTP-7z, since the TME pH is about 6.5, which can just effectively activate PTP-7z. Additionally, as HS attracted more PTP-7z in the presence of Zn^{2+} ions to cell surfaces at pH 6.5 (Figure 10D), it may also increase the extent of the cytotoxicity change of PTP-7z under acidic conditions, which explains the higher pH sensitivity of PTP-7z on cells.

Beyond cell membrane blebbing, for the cells treated with PTP-7z, internalized peptide particles could be observed, especially for those treated with PTP-7z in the presence of Zn^{2+} ions at pH 6.5 (Figure 10D). However, this phenomenon was seldom observed for the cells treated with PTP-7e under all conditions (Figure S12).

The HS-mediated endocytosis of PTP-7z was confirmed by a peptide-lysosome colocalization assay (Figure 11). The results indicate that the peptide PTP-7z was endocytosed by DU145 cancer cells and colocalized with the lysosomes. PTP-7z also formed aggregates within the lysosome, as the arrow pointed (Figure 11A), which confirmed the HS-mediated endocytosis of PTP-7z. Meanwhile, PTP-7e mainly aggregated on the cell membranes (Figure 11B).

As reported by a previous study, HS could mediate nanoparticle endocytosis,[50] and this might be also applied for PTP-7z, suggesting that this peptide may exert other action
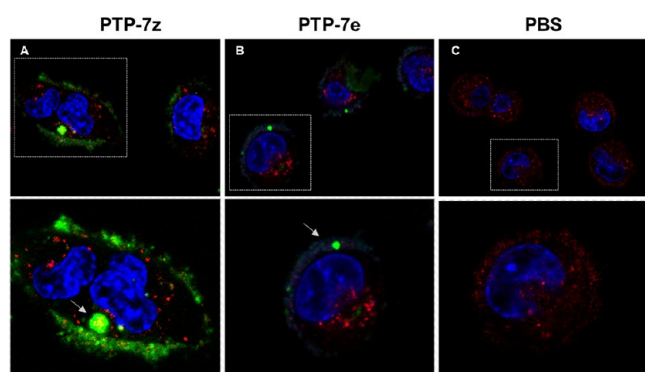
Figure 11. Colocalization of the peptide PTP-7z with the lysosome that was imaged by a laser scanning confocal microscope. (A) PTP-7z-, (B) PTP-7e-, and (C) PBS-treated groups. The peptides PTP-7z and PTP-7e were labeled with FITC, showing green fluorescence. The lysosomes were labeled with the lyso-tracker red probe, and the cell nuclei were labeled with Hoechst 33342 and showed blue fluorescence.

mode besides cell membrane lysis. One of our previously reported anticancer peptides exhibits dual anticancer modes, i.e., cell lysis and pro-apoptosis.[51] Usually, such cationic anticancer peptides would target nucleic acids or mitochondria after internalization due to the positive charges and can induce cell apoptosis. Therefore, we tested peptide-induced cell apoptosis by determining the caspase 3 activity. Caspase 3 is a key zymogen in cell apoptosis and is not activated until it is cleaved by initiator caspases during apoptotic flux.[52] Under the tested conditions (pH 7.4 and 6.5 and adding Zn^{2+} (2 nM)), PTP-7z all showed concentration-dependent proapoptotic activity that was featured as increased caspase 3 activity (Figure 12A–D). The concentration dependence of the proapoptotic activity of PTP-7z should be related to the molecule number that is endocytosed by the cells, whereas

PTP-7e did not show an obvious caspase 3 activity increase. These results indicate that PTP-7z can induce cell apoptosis, but PTP-7e cannot.

The cancer cell killing mechanism of the peptides was also tested by flow cytometry using the Annexin V/PI kit. As demarcated by Krysko et al., during apoptosis, there is a lag time between PS and PI positivities, but in necrosis, these events coincide.[53] PTP-7e showed a typical characteristic of necrosis (Figure 13C,D,G,H), since the cells moved fast from the lower left quadrant (PI-negative/Annexin V-negative cells) to the upper right quadrant of the dot blot (PI-positive/Annexin V-positive cells). Meanwhile, PTP-7z showed both necrosis and apoptosis characteristics, since there were at least 9.30% cells moving to the lower right quadrant, except for the fast movement of cells from the lower left to the upper right quadrant (Figure 13A,B,E,F). These results further confirm the necrosis and apoptosis dual-functional property of PTP-7z and indicate that PTP-7z indeed can induce cell apoptosis after internalization, which can be an alternative way to overcome the glycocalyx barrier to retain anticancer activity.

PTP-7z Inhibits Cancer Cell Migration. HS plays an emerging role in cancer cell migration, and previous studies indicated that HS-instructed peptide self-assembling could inhibit cancer cell migration.[54,55] As the peptide PTP-7z can bind to HS and subsequently self-assemble into large aggregates *in situ*, it may also inhibit cell migration. In the cell scratch repair experiment, low concentrations of the peptides were used to test their inhibition effect on the migration of DU145 cells. At physiological pH (pH 7.4), PTP-7z showed a concentration-dependent inhibition on the wound healing of the cell scratch, which became significant at the concentration of 5 μM (Figure 14A). Addition of Zn^{2+} ions could enhance the inhibitory ability of PTP-7z at a concentration of 5 μM, which is in accordance with the improved HS-binding ability. On the contrary, PTP-7e showed no obvious inhibition on the migration of DU145 cells, even
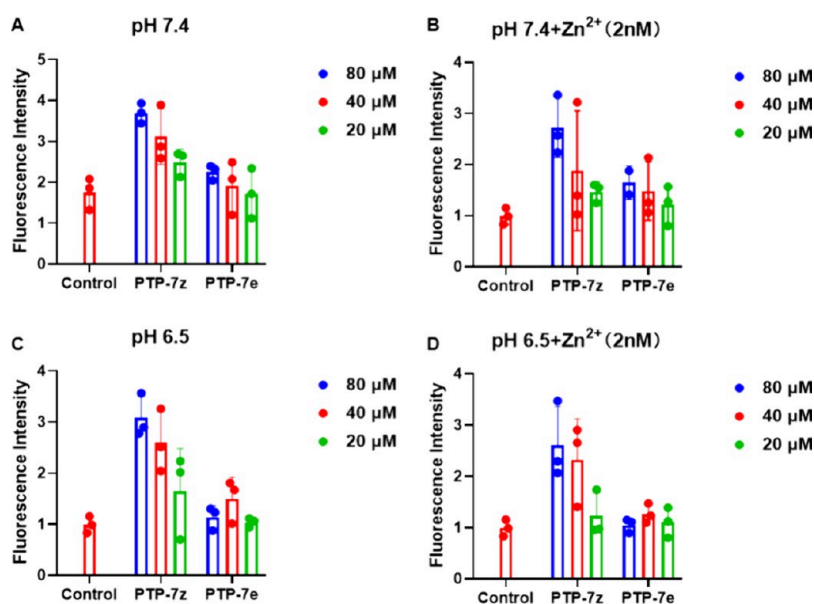
Figure 12. Proapoptotic activity of PTP-7z that was determined by caspase 3 activity. (A) Caspase 3 activity of DU145 cells after treatment with the peptides at pH 7.4. (B) Caspase 3 activity of DU145 cells after treatment with the peptides combined with Zn^{2+} (2 nM) at pH 7.4. (C) Caspase 3 activity of DU145 cells after treatment with the peptides at pH 6.5. (D) Caspase 3 activity of DU145 cells after treatment with the peptides combined with Zn^{2+} (2 nM) at pH 6.5. The caspase 3 activity of DU145 cells after treatment with the peptides was determined by a caspase 3 activity assay kit.
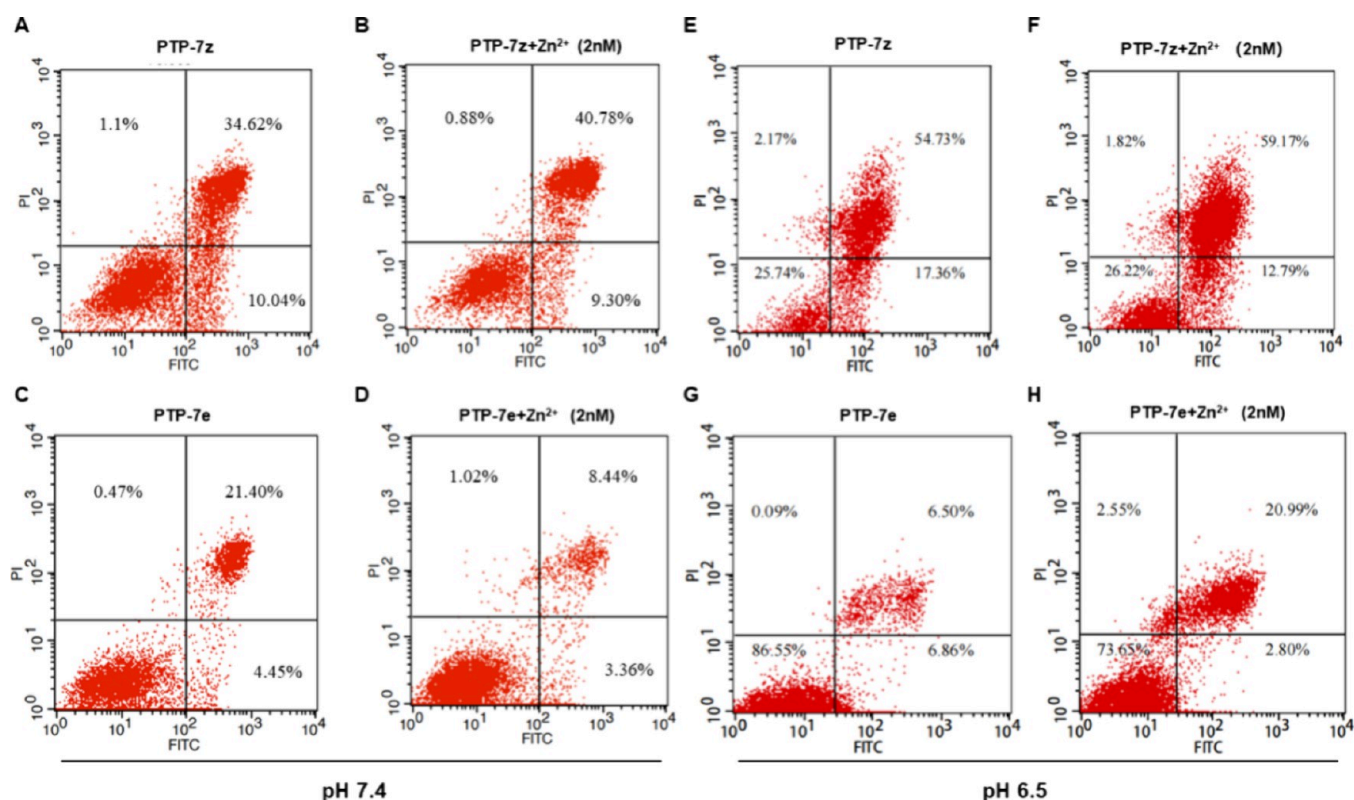
Figure 13. Annexin V-FITC/PI stain and flow cytometry detection of the DU145 cells. (A) PTP-7z-treated group at pH 7.4. (B) PTP-7z combining Zn^{2+} (2 nM)-treated group at pH 7.4. (C) PTP-7e-treated group at pH 7.4. (D) PTP-7e combining Zn^{2+} (2 nM)-treated group at pH 7.4. (E) PTP-7z-treated group at pH 6.5. (F) PTP-7z combining Zn^{2+} (2 nM)-treated group at pH 6.5. (G) PTP-7e-treated group at pH 6.5. (H) PTP-7e combining Zn^{2+} (2 nM)-treated group at pH 6.5. The cells were detected after being treated for 3 h. The peptide concentration used was 40 μM.
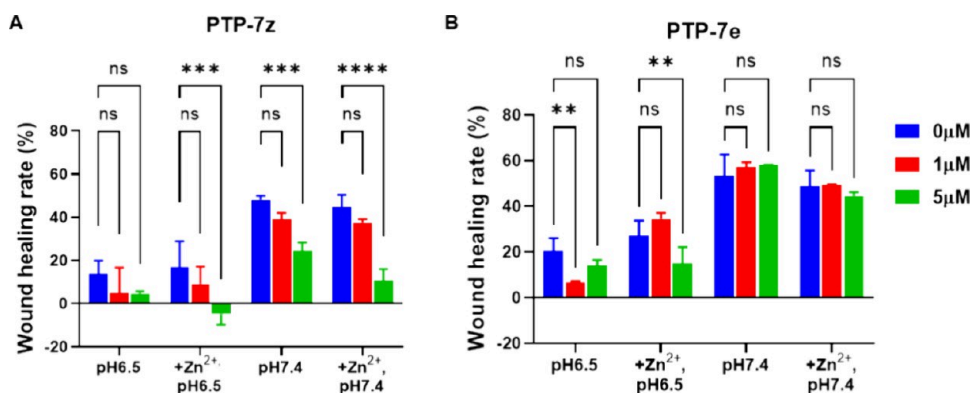
Figure 14. The peptides inhibit cancer cell migration. (A) Cancer cell migration inhibition by PTP-7z under various conditions. (B) Cancer cell migration inhibition by PTP-7e under various conditions. The wound healing rate in 24 h of DU145 cells after the treatment of PTP-7z and PTP-7e under different concentrations (1 and 5 μM) was calculated in a cell scratch assay.

with the addition of Zn^{2+} ions (Figure 14B). This again indicates that the HS-instructed self-assembly of the peptide is important for the inhibitory effect on cancer cell migration. At acidic pH (pH 6.5), cell migration was greatly affected, and both peptides exhibited some inhibition effects on the migration of DU145 cells. Especially, PTP-7z with Zn^{2+} ions even widened the scratch of the cells. Such inhibition effects of these peptides at acidic pH should be related to their pH-activated cytotoxicity, and the cells were killed under this condition. These results extend the anticancer functions of the HS-targeting peptides.

Proposed Self-Delivery and HS-Targeted Anticancer Mechanism of PTP-7z. According to the above results, the anticancer mechanism of PTP-7z can be proposed. With the histidine-rich HS-targeting segment, PTP-7z is able to load Zn^{2+} ions and forms uniform nanoparticles with a diameter of about 50 nm at a low concentration of Zn^{2+} ions (Figure 15A). The improved stability and biosafety ensure efficient self-delivery to the tumor site after injection. The tumor microenvironment is acidic with pH 6.4−7.0,[38] at which the PTP-7z-Zn^{2+} complex can effectively bind to cell surface HS (Figure 15B). Thus, HS further induces the *in situ* self-assembly of PTP-7z to form larger aggregates so as to
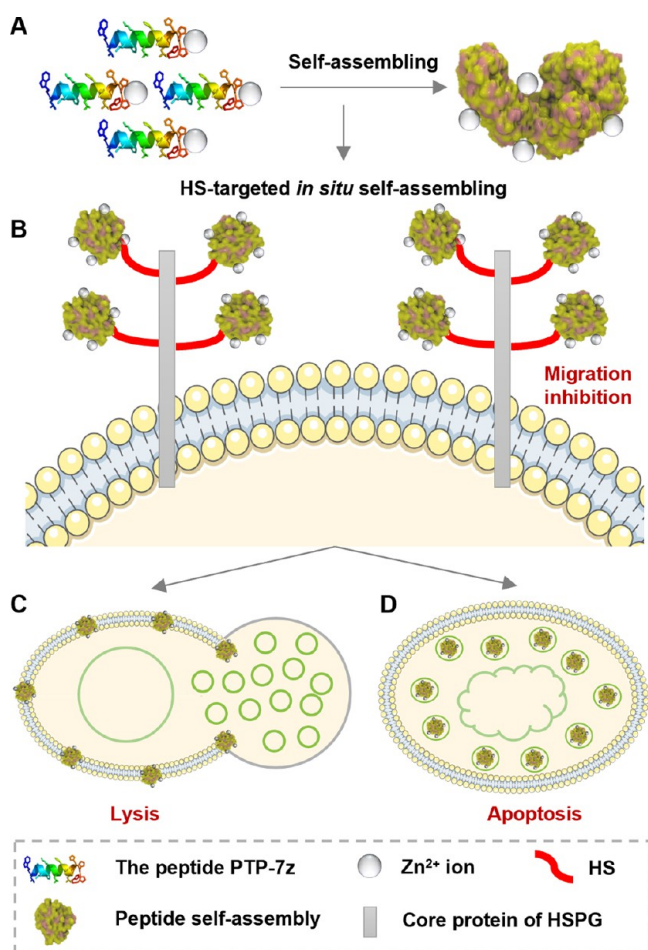
Figure 15. The proposed self-assembling, glycocalyx barrier overcoming and anticancer mechanism of PTP-7z. (A) Self-assembling and self-delivery of the peptide in solution. (B) Acidic pH- and Zn^{2+}-enhanced HS targeting and *in situ* self-assembling of the peptide, which could inhibit the cancer cell migration. (C) The peptide self-assemblies insert and lyse the cancer cell membrane. (D) The peptide self-assemblies are endocytosed and further induce cancer cell apoptosis.

overcome the surface glycocalyx barrier. The peptide PTP-7z then has two destinations to the cancer cells and exerts its anticancer activity. One destination is the cell membranes, and binding of PTP-7z causes the disruption of the lipid bilayer (Figure 15C). The other destination is intracellular targets like mitochondria or mRNA, and binding of PTP-7z may cause cell apoptosis (Figure 15D), as the peptide can translocate into cells through HS-mediated endocytosis and then escape from the endosomes when the pH decreases to 5.5.[56] The dual modes of action of the peptide PTP-7z make it less restricted by the cell surface glycocalyx barrier and maximize its anticancer effects.

CONCLUSIONS

In conclusion, we designed the HS-targeting peptide PTP-7z to overcome the cell surface glycocalyx barrier that may compromise drug activity. When binding to Zn^{2+} ions, PTP-7z could form uniform nanoparticles with an enhanced HS-binding ability and improved serum stability and biosafety. In an acidic tumor microenvironment, HS-induced *in situ* peptide self-assembly further improves the anticancer activity of PTP-7z by promoting cell membrane interaction and intracellular

translocation, rather than hindering the accessibility to the cells. In addition, it can also inhibit cancer cell migration through the HS-induced peptide self-assembling. The sophisticated design of PTP-7z endowed the anticancer lytic peptide with better selectivity, stability, and targetability, which could be extended to other peptide drug design and further proceeded forward to *in vivo* application of such potential anticancer drug candidates.

MATERIALS AND METHODS

Reagents. All peptides (purity, >95%) for this study were commissioned to be synthesized by Genscript (Nanjing, China). Recombinant HSPG was purchased from Cloud-Clone Co. (Wuhan, China). All other reagents if not mentioned were purchased from Sigma Co. (St. Louis, US).

Peptide Structural Prediction and Analysis. The structure of the peptide was predicted by PEP-FOLD3 SERVER (https://mobyle. rpbs.univ-paris-diderot.fr/cgi-bin/portal.py#forms::PEP-FOLD3). The helical wheel projection of the peptide was drawn by Heliquest SERVER (https://heliquest.ipmc.cnrs.fr/cgi-bin/ComputParamsV3. py).

Molecular Dynamics Simulation. Coarse-grained (CG) self-assembling molecular dynamics (MD) simulation of the peptides was performed with the Martini_v2.2 force field on Gromacs 2022.5. The tutorials of Martini high-throughput peptide self-assembly (https:// cgmartini.nl/docs/tutorials/Legacy/martini2/high_throughput.html) and proteins (https://cgmartini.nl/docs/tutorials/Legacy/martini2/ proteins.html) were referenced. Briefly, the PEP-FOLD3-predicted atomistic peptide structures were converted to CG models by the script martinize.py, and 64 CG peptides were placed into a 20 × 20 × 20 nm box. Then, the box was solvated by CG water and neutralized by CG Na^+ and Cl^- ions. After energy minimization and position-restrained MD, the production MD for 9 μs was performed. The self-assembling cluster change during the simulation was analyzed by the gmx clustsize tool. The representative self-assemblies at certain time points were exported by the gmx trjconv tool as pdb files, and the pictures were rendered by VMD (v1.9.3).[57] The Lennard-Jones (LJ) potential and Coulomb potential were analyzed by the gmx energy tool.

Circular Dichroism (CD) Spectra. Peptides were diluted to 20 μM from a stock solution (10 mM, dissolved in 10% v/v DMSO/H_2O) using NaAc buffer (20 mM) at different pH values (7.4 or 5.5), and then the circular dichroism (CD) spectra were detected using a Jasco J-710 spectrometer (Jasco Co.). The scanning conditions were set as follows: start, 240 nm; end, 200 nm; data pitch, 0.2 nm; scanning mode, continuous; scanning speed, 50 nm/min; bandwidth, 1 nm; response, 4 s. A NaAc solution was first added to the CD dish for scanning a baseline, and then different peptides were scanned sequentially. The experiments were performed at room temperature (RT), and the data were averaged from 3 scans, baseline-corrected, smoothed, and exported. The molar specific spin $[\theta]$ was calculated using the following equation:

$$[\theta] = \theta/(L \times nr \times C)$$

where θ is the specific spin, L is the cuvette width, nr is the number of residues, and C is the peptide concentration (in M).

Quenching of the Intrinsic Fluorescence of the Peptides. The peptide solution with a fixed concentration of 40 μM was prepared in 1× PBS (pH 7.4 or 5.5). A zinc ion stock solution (10 mM) was then added to give a final concentration in the range of 0−160 μM. The intrinsic fluorescence of tryptophan (W) residues in the peptides was detected using a multifunctional microplate reader (SpectraMax M2, Molecular Devices),[58] setting the excitation wavelength at 280 nm and the emission wavelength at 350 nm.

ANS Fluorescence Spectra. The 80 μM peptides were prepared in 1 mL of PBS (10 mM) at pH 7.4, 6.5, 6.0, and 5.5 by diluting from the stock solution (10 mM, 10% v/v DMSO). Each tube was vortex-mixed and incubated at 37 °C for 4 h. The ANS stock solution (20

mM, dissolved in DMF) was then added to each tube to give a final concentration of 20 μM. Finally, the solution in each tube was added to a 96-well black-well plate (Beyotime, Shanghai, China) at a concentration of 200 μL per well. Fluorescence detection was performed by using a multifunctional microplate reader (SpectraMax M2, Molecular Devices, USA). The excitation wavelength was set at 369 nm, and the emission wavelength was recorded from 440 to 600 nm. The samples were prepared and tested in triplicate. To test the effects of Zn^{2+} ions, 80 μM peptide solutions of various pH values were added with a $ZnCl_2$ solution to make the final concentration of Zn^{2+} to 2 nM or make the peptide-to-Zn^{2+} concentration ratio to 1:1.

Transmission Electron Microscopy (TEM). Sample solutions were prepared by adding the peptide stock solution to PBS with adjusted pH (7.4, 6.5, and 6.0) to achieve a final concentration of 80 μM and adding Zn^{2+} to make the final concentration of Zn^{2+} to 2 nM or peptide:Zn^{2+} = 1:1. The prepared samples were incubated overnight at 37 °C, and then the peptide sample solutions were added dropwise to the carbon-jetted copper TEM grids and left for deposition for 1 min. After that, the excess peptide solution was removed with filter paper and washed with deionized water. The sample was air-dried for 1 min, and then phosphotungstic acid (2 wt %) was added dropwise and incubated for 2 min for negative staining. The excess staining solution was removed with filter paper, washed with deionized water, and air-dried. Images of the samples were taken with a transmission electron microscope (Hitachi HT7700, Hitachi Ltd., Tokyo, Japan). For the HS-responsive structure transformation assay, after the formation of the assemblies as before, the HS stock solution (25 mg/mL) was added to make the final concentration of 250 μg/mL, and the mixture was incubated for 2 h.

Surface Plasmon Resonance (SPR) Experiments. The binding ability of peptides to HSPG was determined on a dual-channel SPR instrument (OpenSPR, NICOYA, Canada). HSPG syndecan proteoglycan 2 was first fixed to the high-sensitivity carboxylate chip of channel 2 in PBS buffer at pH 7.4, and then channel 1 was blocked with ethanolamine. Isopropanol (80%) was used to evacuate bubbles and equilibrate the system, and then the peptide samples of different concentrations (100, 50, and 10 μM) were injected into the system. After each injection, the system was washed, evacuated, and equilibrated again. After the tests at pH 7.4, the buffer was switched to PBS at pH 6.5 and 6.0, the bubble evacuation and system equilibration procedures were repeated, and the peptide samples of different concentrations (100, 50, and 10 μM) were loaded again. Finally, the buffer was changed to PBS containing 2 nM Zn^{2+} at pH 7.4, 6.5, and 6.0 to determine the effects of Zn^{2+} on the peptide-HS binding. After the tests were completed, the binding kinetics and affinity data were evaluated with data analysis software (Trance-Drewer 1.9.2).

Zeta Potential Measurements. Peptides from stock solutions (10 mM, 10% DMSO) were diluted with deionized water of various pH values (7.4, 7.0, 6.5, 6.0, and 5.5) to 40 μM for two groups. The second group was added with $ZnCl_2$ to make the Zn^{2+}/peptide ratio to 1.0. Freshly prepared peptide solutions were subjected to a brief (60 s) sonication treatment, and then the zeta potentials of the peptide solutions were measured immediately using a Malvern Zetasizer Nano ZS90 (Malvern Instruments Ltd., U.K.).

Cell Culture. DU145, A549, and HUVEC cell lines were obtained from the Cell Resource Center, Peking Union Medical College (which is part of the National Science and Technology Infrastructure, the National Biomedical Cell-Line Resource, NSTI-BMCR; http://cellresource.cn). DU145 was cultured in RPMI-1640 medium (Corning, catalog number: 10-040-CV) that contained 10% fetal bovine serum (FBS, ExCell, catalog number: FSP500) and 1% penicillin—streptomycin (10,000 U/mL, Gibco, catalog number: 15140122) and incubated in a humidified atmosphere of 5% CO_2 at 37 °C. The A549 cells were cultured in F-12K media (Gibco, catalog number: 21127022), and the HUVEC cells were cultured in DMEM medium (Corning, catalog number: 10-013-CV).

Cytotoxicity Assay. Peptide cytotoxicity was determined by an MTT assay. Briefly, cell suspensions in complete medium were added to 96-well plates (5×10^3 cells per well) after digestion with trypsin

and incubated overnight at 37 °C to allow the cells to adhere to the bottom of the wells. Then, the medium was changed to fresh medium containing different concentrations of peptides with or without Zn^{2+} ions, and the mixture was incubated for 24 h. After incubation, 100 μL of MTT (0.5 mg/mL) diluted with the cell medium was added to each well. After another 4 h of incubation, 100 μL of triple lysate (10% SDS solution containing 5% isopropyl alcohol and 0.1% HCl) was added to each well and placed at 37 °C for 4 h to dissolve the crystallized MTT. The absorbance at 570 nm was measured using a multifunctional microplate reader (SpectraMax M2, Molecular Devices) to calculate cell viability, and finally, the IC_{50} value was fitted.

Immunofluorescence Staining and Cellular Imaging. DU145 cell suspensions with a density of 10^5 cells/mL were inoculated into eight-well chamber slides (Thermo Scientific, catalog number: 177402) at 500 μL per well and placed in an incubator overnight for cell attachment. The medium was discarded, and the cells were washed with PBS. Subsequently, staining was performed as follows: (1) 200 μL of 1:500 diluted mouse anti-HS antibody (10E4 epitope, USBiological, catalog number: H1890) was added as a primary antibody, incubated at 37 °C for 1 h, and then aspirated and washed; (2) 200 μL of 1:500 dilution of secondary antibody with Cy3 fluorescent labeling (A0521, Beyotime, China) was added, incubated at 37 °C for 1 h, and then washed; (3) a 200 μL DAPI staining solution (C1005, Beyotime, China) was added, incubated at 37 °C for 10 min, and then aspirated and washed; (4) a 200 μL peptide solution with FITC labeling (10 μM) was added and incubated for 30 min or 2 h. The stained cell images were observed and captured by confocal laser scanning microscopy (CLSM) (TCS SP8, Leica Microsystems). The excitation wavelengths used were 405, 488, and 550 nm, and the emission center wavelengths of DAPI, FITC, and Cy3 were chosen to be 454, 520, and 570 nm, respectively.

Caspase 3 Activity Test Assay. DU145 cells were seeded at 8000 cells per well in a sterile 96-well black plate and incubated overnight. The stock solution of PTP-7z and PTP-7e was diluted with serum-free media at pH 7.4 and 6.5 to 20, 40, and 80 μM as the peptide-only groups. On the basis of the peptide-only groups, a $ZnCl_2$ (10 mM) solution was added to form the peptide + Zn^{2+} (2 nM) groups. After the old culture medium was aspirated, the peptide solutions were added into the black plate and incubated for 3 h. The serum-free medium and the medium with Zn^{2+} (2 nM) at different pH values were used as controls. Subsequently, the peptide solution was discarded, and the cells were treated with a GreenNuc Caspase-3 Assay Kit for Live Cells (Beyotime, C1168S, Shanghai, China) for 30 min. The fluorescence was measured with a microplate reader (SpectraMax M2, Molecular Devices) with an excitation wavelength of 485 nm and an emission wavelength of 515 nm.

Peptide-Lysosome Colocalization Detection. DU145 cells were seeded in a confocal dish at 40,000 cells per well and incubated overnight. After aspirating the old culture medium, a Hoechst 33342 live cell staining solution (Solarbio, C0031, Beijing, China) was added and incubated for 5 min to stain the nuclei. Then, FITC-labeled PTP-7e/PTP-7z at a concentration of 5 μM was added and incubated for 30 min, while the control group was treated with PBS at the same time. Subsequently, the lysosomes were stained with Lyso-Tracker Red (Solarbio, L8010, Beijing, China), a lysosome-targeting red fluorescent probe, for 30 min. After the removal of the staining solution, fresh cell culture medium was added. The cells were observed and imaged by CLSM (TCS SP8, Leica Microsystems).

Flow Cytometry. The DU145 cell suspensions with a density of 10^5 cells/mL were inoculated into a 12-well plate and incubated overnight, then the old medium was discarded, and the cells were washed with PBS. For the peptide-only group, the peptide stock solution (10 mM, 10% DMSO) was diluted with serum-free medium at pH 7.4 and 6.5 to 40 μM, then added to the wells, and incubated for 3 h. The serum-free medium was added as a control. For the peptide + Zn^{2+} group, a Zn^{2+} solution was added to the serum-free medium to the final concentration of 2 nM, and then the peptide stock solution was diluted as before to treat the cells. The serum-free medium containing 2 nM Zn^{2+} was added as a control. Three hours

later, the cells were digested with 0.25% trypsin (without EDTA) for 2 min. The digestion was stopped by complete medium, and the sample was centrifuged at 1000g to collect the cells. The cells were resuspended with 2 mL of PBS and centrifuged again, stained with an Annexin V-FITC/PI apoptosis kit (Beyotime, catalog number: C1062S), and detected by a flow cytometer (BD FACSCalibur). The data were analyzed by FlowJo software.

Wound Healing Assay. The DU145 cell suspension was added to a 6-well plate (2×10^5 per well). After the cells attached to the bottom of the well, a line was drawn in the middle of the well. The old medium was discarded and washed with PBS to remove the unattached cells. Then, the peptide solutions at pH 7.4 and 6.5, as the peptide-only group or peptide + Zn^{2+} (2 nM) group, at concentrations of 1 and 5 μM in serum-free medium, were added to the wells. The media at pH 7.4 and 6.5 were set as controls. The pictures of the line were taken by a microscope (Optec BDS400) with a digital camera before the peptide addition (as 0 h) and after the peptide addition for 24 h, with ×400 magnification, and 3 pictures of each line were taken. The pictures were analyzed by the plugin MRI_Wound_Healing_Tool of ImageJ to calculate the area (A), and the wound healing rate was calculated by the equation:

$$\text{wound healing rate } (\%) = (1 - A_{24h}/A_{0h}) \times 100$$

Peptide Stability in Serum. The peptide stock solution (10 mM) was diluted to 200 μM with 10% FBS and incubated in an incubator at 37 °C. At different time points (0, 0.5, 2, 3, and 5 h), a 50 μL solution was withdrawn and mixed with 5 times volume of acetonitrile to remove serum proteins. The solution was centrifuged at 4 °C and 12,000 rpm for 5 min, and the supernatant was collected and analyzed by HPLC (Agilent, 1260 Infinity II) with a C18 column (Agilent HC-C18(2)). The peptide peak area was then integrated and divided with the area of the control (not treated with FBS) to obtain the proportional percentage of the remaining peptides. The half-lives were fitted with a one-phase decay algorithm.

Hemolysis Experiments. Mouse blood was collected in vacuum blood collection tubes containing EDTA, then the blood samples were centrifuged at 1500 rpm at 4 °C for 5 min, the supernatant was discarded and washed with saline, and centrifugation was repeated three times. Then, the precipitated erythrocytes were resuspended in a volume of PBS equal to that of the original blood, and the obtained RBC suspension was kept on ice and prepared for hemolysis assay. Stock solutions of peptides PTP-7e and PTP-7z were first diluted to a range of concentrations in 800 μL volume of PBS. Prepared RBC suspensions (200 μL) were then added to the peptide solutions to give final peptide concentrations of 31.25, 62.5, 125, 250, and 500 μM in the absence or presence of Zn^{2+} ions (2 nM). Erythrocytes in PBS and deionized water were used as 0 and 100% lysis controls, respectively. The mixtures were inverted several times to mix and incubated in an incubator at 37 °C for 1 h. Finally, the samples were centrifuged at 13,500 rpm for 5 min, the supernatant was aspirated, and the absorbance was measured at 541 nm. The hemolysis rate of erythrocytes was calculated by the equation:

$$\text{hemolysis rate } (\%) = (A - A_0)/(A_{100} - A_0) \times 100$$

where A, A_0, and A_{100} are the absorbance at 541 nm of the sample, 0% hemolysis solution, and 100% hemolysis solution, respectively. All samples were tested in triplicate.

Statistical Analysis. Statistical analysis was performed with Prism 8 (GraphPad Software). The measurement data were expressed as the mean ± standard deviation (SD). One-way ANOVA was applied to compare differences between the experimental and control groups. Student's t test was used for the comparison between two groups.

■ ASSOCIATED CONTENT

Ⓢ Supporting Information

The Supporting Information is available free of charge at https://pubs.acs.org/doi/10.1021/acsami.4c09243.

Intrinsic fluorescence quenching and CD spectra of the peptides; cytotoxicity curve of the peptides; *in vivo* stability and safety by the Zn^{2+}-enhanced peptide self-assembling; targeting, *in situ* self-assembling with HS, and membrane lysis of PTP-7e (PDF)

■ AUTHOR INFORMATION

Corresponding Authors

Long Chen − *State Key Laboratory of Chemical Resource Engineering, College of Life Science and Technology, Beijing University of Chemical Technology, Beijing 100029, China;* ⓞ orcid.org/0000-0002-3812-1815; Email: chenlong@mail.buct.edu.cn

Chuanke Zhao − *Key Laboratory of Carcinogenesis and Translational Research (Ministry of Education/Beijing), Department of Biochemistry and Molecular Biology, Peking University Cancer Hospital & Institute, Beijing 100142, China;* Email: zhaochk@bjmu.edu.cn

Jun F. Liang − *Department of Chemistry, Chemical Biology, and Biomedical Engineering, Stevens Institute of Technology, Hoboken, New Jersey 07030, United States;* Email: jliang2@stevens.edu

Shi-Zhong Luo − *State Key Laboratory of Chemical Resource Engineering, College of Life Science and Technology, Beijing University of Chemical Technology, Beijing 100029, China;* Email: luosz@mail.buct.edu.cn

Authors

Pengfei Pei − *State Key Laboratory of Chemical Resource Engineering, College of Life Science and Technology, Beijing University of Chemical Technology, Beijing 100029, China*

Xinyao Guan − *State Key Laboratory of Chemical Resource Engineering, College of Life Science and Technology, Beijing University of Chemical Technology, Beijing 100029, China*

Peng Wei − *School of Traditional Chinese Medicine, Beijing University of Chinese Medicine, Beijing 102488, China;* ⓞ orcid.org/0000-0002-3721-7014

Xiaoxu Kang − *Institute of Medical Science, China-Japan Friendship Hospital, Beijing 100029, China*

Lili Gong − *Institute of Medical Science, China-Japan Friendship Hospital, Beijing 100029, China;* ⓞ orcid.org/0000-0002-0061-2029

Lihong Liu − *Institute of Medical Science, China-Japan Friendship Hospital, Beijing 100029, China*

Wenxu Guo − *State Key Laboratory of Chemical Resource Engineering, College of Life Science and Technology, Beijing University of Chemical Technology, Beijing 100029, China*

Renji Gu − *State Key Laboratory of Chemical Resource Engineering, College of Life Science and Technology, Beijing University of Chemical Technology, Beijing 100029, China*

Lixin Wang − *Key Laboratory of Carcinogenesis and Translational Research (Ministry of Education/Beijing), Department of Biochemistry and Molecular Biology, Peking University Cancer Hospital & Institute, Beijing 100142, China*

Complete contact information is available at:
https://pubs.acs.org/10.1021/acsami.4c09243

Author Contributions

#P.P., L.C., and X.G. contributed equally to this work.

Notes

The authors declare no competing financial interest.

REFERENCES

(1) Kuo, J. C. H.; Gandhi, J. G.; Zia, R. N.; Paszek, M. J. Physical biology of the cancer cell glycocalyx. *Nat. Phys.* **2018**, *14* (7), 658−669.

(2) Fadnes, B.; Rekdal, O.; Uhlin-Hansen, L. The anticancer activity of lytic peptides is inhibited by heparan sulfate on the surface of the tumor cells. *BMC Cancer* **2009**, *9*, 183.

(3) Fadnes, B.; Uhlin-Hansen, L.; Lindin, I.; Rekdal, Ø. Small lytic peptides escape the inhibitory effect of heparan sulfate on the surface of cancer cells. *BMC Cancer* **2011**, *11*, 116.

(4) Chen, L. *Dual-directional improvement of cancer treatment.* Stevens Institute of Technology, 2013.

(5) Couchman, J. R. Syndecans: proteoglycan regulators of cell-surface microdomains? *Nat. Rev. Mol. Cell Biol.* **2003**, *4* (12), 926−37.

(6) Bishop, J. R.; Schuksz, M.; Esko, J. D. Heparan sulphate proteoglycans fine-tune mammalian physiology. *Nature* **2007**, *446* (7139), 1030−7.

(7) Xue, S.; Zhou, F.; Zhao, T.; Zhao, H.; Wang, X.; Chen, L.; Li, J. P.; Luo, S. Z. Phase separation on cell surface facilitates bFGF signal transduction with heparan sulphate. *Nat. Commun.* **2022**, *13* (1), 1112.

(8) Crublet, E.; Andrieu, J. P.; Vives, R. R.; Lortat-Jacob, H. The HIV-1 envelope glycoprotein gp120 features four heparan sulfate binding domains, including the co-receptor binding site. *J. Biol. Chem.* **2008**, *283* (22), 15193−200.

(9) Hu, Y.; Meng, X.; Zhang, F.; Xiang, Y.; Wang, J. The in vitro antiviral activity of lactoferrin against common human coronaviruses and SARS-CoV-2 is mediated by targeting the heparan sulfate co-receptor. *Emerg Microbes Infect* **2021**, *10* (1), 317−330.

(10) Dechecchi, M. C.; Melotti, P.; Bonizzato, A.; Santacatterina, M.; Chilosi, M.; Cabrini, G. Heparan sulfate glycosaminoglycans are receptors sufficient to mediate the initial binding of adenovirus types 2 and 5. *J. Virol* **2001**, *75* (18), 8772−80.

(11) Kalia, M.; Chandra, V.; Rahman, S. A.; Sehgal, D.; Jameel, S. Heparan sulfate proteoglycans are required for cellular binding of the hepatitis E virus ORF2 capsid protein and for viral infection. *J. Virol* **2009**, *83* (24), 12714−24.

(12) Clausen, T. M.; Sandoval, D. R.; Spliid, C. B.; Pihl, J.; Perrett, H. R.; Painter, C. D.; Narayanan, A.; Majowicz, S. A.; Kwong, E. M.; McVicar, R. N.; Thacker, B. E.; Glass, C. A.; Yang, Z.; Torres, J. L.; Golden, G. J.; Bartels, P. L.; Porell, R. N.; Garretson, A. F.; Laubach, L.; Feldman, J.; Yin, X.; Pu, Y.; Hauser, B. M.; Caradonna, T. M.; Kellman, B. P.; Martino, C.; Gordts, P. L. S. M.; Chanda, S. K.; Schmidt, A. G.; Godula, K.; Leibel, S. L.; Jose, J.; Corbett, K. D.; Ward, A. B.; Carlin, A. F.; Esko, J. D. SARS-CoV-2 Infection Depends on Cellular Heparan Sulfate and ACE2. *Cell* **2020**, *183* (4), 1043−1057.e15.

(13) Liu, L.; Chopra, P.; Li, X.; Bouwman, K. M.; Tompkins, S. M.; Wolfert, M. A.; de Vries, R. P.; Boons, G.-J. Heparan Sulfate Proteoglycans as Attachment Factor for SARS-CoV-2. *ACS Central Science* **2021**, *7* (6), 1009−1018.

(14) Park, S.; Colville, M. J.; Paek, J. H.; Shurer, C. R.; Singh, A.; Secor, E. J.; Sailer, C. J.; Huang, L. T.; Kuo, J. C.; Goudge, M. C.; Su, J.; Kim, M.; DeLisa, M. P.; Neelamegham, S.; Lammerding, J.; Zipfel, W. R.; Fischbach, C.; Reesink, H. L.; Paszek, M. J. Immunoengineering can overcome the glycocalyx armour of cancer cells. *Nat. Mater.* **2024**, *23* (3), 429−438.

(15) Ziegler, A.; Nervi, P.; Durrenberger, M.; Seelig, J. The cationic cell-penetrating peptide CPP(TAT) derived from the HIV-1 protein TAT is rapidly transported into living fibroblasts: optical, biophysical, and metabolic evidence. *Biochemistry* **2005**, *44* (1), 138−48.

(16) Snow, A. D.; Cummings, J. A.; Lake, T. The Unifying Hypothesis of Alzheimer's Disease: Heparan Sulfate Proteoglycans/Glycosaminoglycans Are Key as First Hypothesized Over 30 Years Ago. *Front Aging Neurosci* **2021**, *13*, No. 710683.

(17) Holmes, B. B.; DeVos, S. L.; Kfoury, N.; Li, M.; Jacks, R.; Yanamandra, K.; Ouidja, M. O.; Brodsky, F. M.; Marasa, J.; Bagchi, D. P.; Kotzbauer, P. T.; Miller, T. M.; Papy-Garcia, D.; Diamond, M. I. Heparan sulfate proteoglycans mediate internalization and propagation of specific proteopathic seeds. *Proc. Natl. Acad. Sci. U. S. A.* **2013**, *110* (33), E3138−E3147.

(18) Wang, Z.; Zhao, C.; Li, Y.; Wang, J.; Hou, D.; Wang, L.; Wang, Y.; Wang, X.; Liu, X.; Wang, H.; Xu, W. Photostable Cascade-Activatable Peptide Self-Assembly on a Cancer Cell Membrane for High-Performance Identification of Human Bladder Cancer. *Adv. Mater.* **2023**, *35* (35), No. e2210732.

(19) Chen, L.; Patrone, N.; Liang, J. F. Peptide self-assembly on cell membranes to induce cell lysis. *Biomacromolecules* **2012**, *13* (10), 3327−33.

(20) Pei, P.; Chen, L.; Fan, R.; Zhou, X. R.; Feng, S.; Liu, H.; Guo, Q.; Yin, H.; Zhang, Q.; Sun, F.; Peng, L.; Wei, P.; He, C.; Qiao, R.; Wang, Z.; Luo, S. Z. Computer-Aided Design of Lasso-like Self-Assembling Anticancer Peptides with Multiple Functions for Targeted Self-Delivery and Cancer Treatments. *ACS Nano* **2022**, *16* (9), 13783−13799.

(21) Sun, F.; Ding, X.; Xu, L.; Liang, J. F.; Chen, L.; Luo, S.-Z. A Molecular Dynamics Study of the Short-Helical-Cytolytic Peptide Assembling and Bioactive on Membrane Interface. *J. Phys. Chem. C* **2017**, *121* (32), 17263−17275.

(22) Ge, X.; Cao, Y.; Zhu, X.; Yuan, B.; He, L.; Wu, A.; Li, J. Self-Assembly of Organelle-Localized Neuropeptides Triggers Intrinsic Apoptosis Against Breast Cancer. *Adv. Healthcare Mater.* **2023**, *12* (25), No. e2300265.

(23) Borza, D.-B.; Morgan, W. T. Histidine-Proline-rich Glycoprotein as a Plasma pH Sensor. *THE JOURNAL OF BIOLOGICAL CHEMISTRY* **1998**, *273* (6), 5493−5499.

(24) Lamiable, A.; Thevenet, P.; Rey, J.; Vavrusa, M.; Derreumaux, P.; Tuffery, P. PEP-FOLD3: faster de novo structure prediction for linear peptides in solution and in complex. *Nucleic Acids Res.* **2016**, *44* (W1), W449−54.

(25) Monticelli, L.; Kandasamy, S. K.; Periole, X.; Larson, R. G.; Tieleman, D. P.; Marrink, S. J. The MARTINI Coarse-Grained Force Field: Extension to Proteins. *J. Chem. Theory Comput* **2008**, *4* (5), 819−34.

(26) Sontz, P. A.; Song, W. J.; Tezcan, F. A. Interfacial metal coordination in engineered protein and peptide assemblies. *Curr. Opin Chem. Biol.* **2014**, *19*, 42−9.

(27) Liao, S. M.; Du, Q. S.; Meng, J. Z.; Pang, Z. W.; Huang, R. B. The multiple roles of histidine in protein interactions. *Chem. Cent. J.* **2013**, *7* (1), 44.

(28) Laitaoja, M.; Valjakka, J.; Janis, J. Zinc coordination spheres in protein structures. *Inorg. Chem.* **2013**, *52* (19), 10983−91.

(29) Laity, J. H.; Lee, B. M.; Wright, P. E. Zinc finger proteins: new insights into structural and functional diversity. *Curr. Opin. Struct. Biol.* **2001**, *11* (1), 39−46.

(30) Priebatsch, K. M.; Kvansakul, M.; Poon, I. K.; Hulett, M. D. Functional Regulation of the Plasma Protein Histidine-Rich Glycoprotein by Zn(2+) in Settings of Tissue Injury. *Biomolecules* **2017**, *7* (1), 22.

(31) Hutchens, T. W.; Yip, T. T. Synthetic metal-binding protein surface domains for metal ion-dependent interaction chromatography. II. Immobilization of synthetic metal-binding peptides from metal ion

transport proteins as model bioactive protein surface domains. *J. Chromatogr.* **1992**, *604* (1), 133−41.

(32) Bruch, M. D.; Hoyt, D. W. Conformational analysis of a mitochondrial presequence derived from the F1-ATPase beta-subunit by CD and NMR spectroscopy. *Biochim. Biophys. Acta* **1992**, *1159* (1), 81−93.

(33) Hoang, T.; Kuljanin, M.; Smith, M. D.; Jelokhani-Niaraki, M. A biophysical study on molecular physiology of the uncoupling proteins of the central nervous system. *Biosci. Rep.* **2015**, *35* (4), No. e00226.

(34) Zhou, X. R.; Cao, Y.; Zhang, Q.; Tian, X. B.; Dong, H.; Chen, L.; Luo, S. Z. Self-assembly nanostructure controlled sustained release, activity and stability of peptide drugs. *Int. J. Pharm.* **2017**, *528* (1−2), 723−731.

(35) Chen, L.; Tu, Z.; Voloshchuk, N.; Liang, J. F. Lytic peptides with improved stability and selectivity designed for cancer treatment. *J. Pharm. Sci.* **2012**, *101* (4), 1508−17.

(36) Chen, W. T.; Liao, Y. H.; Yu, H. M.; Cheng, I. H.; Chen, Y. R. Distinct effects of Zn2+, Cu2+, Fe3+, and Al3+ on amyloid-beta stability, oligomerization, and aggregation: amyloid-beta destabilization promotes annular protofibril formation. *J. Biol. Chem.* **2011**, *286* (11), 9646−56.

(37) Younan, N. D.; Viles, J. H. A Comparison of Three Fluorophores for the Detection of Amyloid Fibers and Prefibrillar Oligomeric Assemblies. ThT (Thioflavin T); ANS (1-Anilinonaph-thalene-8-sulfonic Acid); and bisANS (4,4'-Dianilino-1,1'-binaphthyl-5,5'-disulfonic Acid). *Biochemistry* **2015**, *54* (28), 4297−306.

(38) Boedtkjer, E.; Pedersen, S. F. The Acidic Tumor Micro-environment as a Driver of Cancer. *Annu. Rev. Physiol.* **2020**, *82*, 103−126.

(39) Anderson, M.; Moshnikova, A.; Engelman, D. M.; Reshetnyak, Y. K.; Andreev, O. A. Probe for the measurement of cell surface pH in vivo and ex vivo. *Proc. Natl. Acad. Sci. U. S. A.* **2016**, *113* (29), 8177−8181.

(40) Gasymov, O. K.; Glasgow, B. J. ANS fluorescence: potential to augment the identification of the external binding sites of proteins. *Biochim. Biophys. Acta* **2007**, *1774* (3), 403−11.

(41) Guliyeva, A. J.; Gasymov, O. K. ANS fluorescence: Potential to discriminate hydrophobic sites of proteins in solid states. *Biochem Biophys Rep* **2020**, *24*, No. 100843.

(42) Matulis, D.; Lovrien, R. 1-Anilino-8-Naphthalene Sulfonate Anion-Protein Binding Depends Primarily on Ion Pair Formation. *Biophys. J.* **1998**, *74* (1), 422−429.

(43) Yang, J.; An, H. W.; Wang, H. Self-Assembled Peptide Drug Delivery Systems. *ACS Appl. Bio Mater.* **2021**, *4* (1), 24−46.

(44) Park, J. H.; Oh, N. Endocytosis and exocytosis of nanoparticles in mammalian cells. *Int. J. Nanomed.* **2014**, 51.

(45) Geng, Y.; Dalhaimer, P.; Cai, S.; Tsai, R.; Tewari, M.; Minko, T.; Discher, D. E. Shape effects of filaments versus spherical particles in flow and drug delivery. *Nat. Nanotechnol.* **2007**, *2* (4), 249−255.

(46) Magneson, G. R.; Puvathingal, J. M.; Ray, W. J. The concentrations of free Mg2+ and free Zn2+ in equine blood plasma. *J. Biol. Chem.* **1987**, *262* (23), 11140−11148.

(47) Suhovskih, A. V.; Domanitskaya, N. V.; Tsidulko, A. Y.; Prudnikova, T. Y.; Kashuba, V. I.; Grigorieva, E. V. Tissue-specificity of heparan sulfate biosynthetic machinery in cancer. *Cell Adh Migr* **2015**, *9* (6), 452−9.

(48) Babiychuk, E. B.; Monastyrskaya, K.; Potez, S.; Draeger, A. Blebbing confers resistance against cell lysis. *Cell Death & Differentiation* **2011**, *18* (1), 80−89.

(49) Zhang, Y.; Chen, X.; Gueydan, C.; Han, J. Plasma membrane changes during programmed cell deaths. *Cell Research* **2018**, *28* (1), 9−21.

(50) Mandarini, E.; Tollapi, E.; Zanchi, M.; Depau, L.; Pini, A.; Brunetti, J.; Bracci, L.; Falciani, C. Endocytosis and Trafficking of Heparan Sulfate Proteoglycans in Triple-Negative Breast Cancer Cells Unraveled with a Polycationic Peptide. *Int. J. Mol. Sci.* **2020**, *21* (21), 8282.

(51) Zhou, X. R.; Zhang, Q.; Tian, X. B.; Cao, Y. M.; Liu, Z. Q.; Fan, R.; Ding, X. F.; Zhu, Z.; Chen, L.; Luo, S. Z. From a pro-apoptotic peptide to a lytic peptide: One single residue mutation. *Biochim. Biophys. Acta* **2016**, *1858* (8), 1914−25.

(52) Porter, A. G.; Jänicke, R. U. Emerging roles of caspase-3 in apoptosis. *Cell Death & Differentiation* **1999**, *6* (2), 99−104.

(53) Krysko, D. V.; Vanden Berghe, T.; D'Herde, K.; Vandenabeele, P. Apoptosis and necrosis: Detection, discrimination and phagocy-tosis. *Methods* **2008**, *44* (3), 205−221.

(54) Roy, S. R.; Li, G.; Hu, X.; Zhang, S.; Yukawa, S.; Du, E.; Zhang, Y. Integrin and Heparan Sulfate Dual-Targeting Peptide Assembly Suppresses Cancer Metastasis. *ACS Appl. Mater. Interfaces* **2020**, *12* (17), 19277−19284.

(55) Mang, D.; Roy, S. R.; Zhang, Q.; Hu, X.; Zhang, Y. Heparan Sulfate-Instructed Self-Assembly Selectively Inhibits Cancer Cell Migration. *ACS Appl. Mater. Interfaces* **2021**, *13* (15), 17236−17242.

(56) Sahni, A.; Qian, Z.; Pei, D. Cell-Penetrating Peptides Escape the Endosome by Inducing Vesicle Budding and Collapse. *ACS Chem. Biol.* **2020**, *15* (9), 2485−2492.

(57) Humphrey, W.; Dalke, A.; Schulten, K. VMD: visual molecular dynamics. *J. Mol. Graph* **1996**, *14* (1), 33−8.

(58) Zirah, S.; Kozin, S. A.; Mazur, A. K.; Blond, A.; Cheminant, M.; Segalas-Milazzo, I.; Debey, P.; Rebuffat, S. Structural changes of region 1−16 of the Alzheimer disease amyloid beta-peptide upon zinc binding and in vitro aging. *J. Biol. Chem.* **2006**, *281* (4), 2151−61.